NEW PERSPECTIVES ON LUNAR VOLCANISM

A THESIS SUBMITTED TO THE GRADUATE DIVISION OF THE UNIVERSITY OF HAWAII IN PARTIAL FULFILLMENT OF THE REQUIREMENTS FOR THE DEGREE OF

MASTER OF SCIENCE

IN

GEOLOGY AND GEOPHYSICS

December 2001

By
Thomas A. Giguere

Thesis Committee:

G. Jeffrey Taylor, Chairperson
B. Ray Hawke
Paul G. Lucey

We certify that we have read this thesis and that, in our opinion, it is satisfactory in scope and quality as a thesis for the degree of Master of Science in Geology And Geophysics (Planetary Geosciences And Remote Sensing).

THESIS COMMITTEE

Chairperson

Bernard Ray Hawke

Paul Lucey

ABSTRACT

Lunar mare basalt sample data suggest that there is a bimodal distribution of TiO_2 concentrations. Using a refined technique for remote determination of TiO_2, we find that the maria actually vary continuously from low to high values. The nine lunar sample return missions were not situated near intermediate basalt regions. Maria with 2-4 wt. % TiO_2 are most abundant, and abundance decreases with increasing TiO_2. Maria surfaces with TiO_2 >5 wt. % constitute only 20% of the maria. The distribution of basalt Ti contents probably reflects both the relative abundances of ilmenite-free and ilmenite-bearing mantle sources. This distribution is consistent with models of the formation of mare source regions as cumulates from the lunar magma ocean.

Several dark-haloed and dark-rayed craters have been identified in the Maurolycus region in the southeastern nearside highlands. Multispectral imagery were used to investigate the composition and origin of dark-haloed craters in the region. A striking albedo anomaly is associated with Buch B crater which exhibits both a dark halo and dark rays. Buch B is an impact structure, not a volcanic vent. FeO and TiO_2 data as well as five point spectra images indicate that the dark ejecta is composed of immature mare-like material and may contain minor amounts of highland debris. Buch B excavated either an isolated cryptomare or much more likely, a mafic intrusion, such as a dike of basaltic composition.

The Lomonosov-Fleming region was examined with the Clementine five-color UV-VIS digital image model. Dark halo craters have been identified and mapped, and were confirmed to be exogenically produced. Spectra confirm that the dark halos were produced by the excavation of dark, mafic material from beneath a higher-albedo surface. FeO and TiO_2 values have been reduced by contamination from nearby highland material; nonetheless, selected TiO_2 values are higher in the Lomonosov-Fleming region than in any other cryptomare. Mare surface units in the Lomonosov-Fleming region are small and appear to be contaminated by highlands material. There following mechanisms contributed to the formation of the cryptomare: 1) ancient mare surfaces were covered with varying thicknesses of highlands debris, 2) both impact basins and craters played a role by transporting highlands material to mare surfaces, and 3) Humboldtianum basin may have implaced basin-ejecta material.

TABLE OF CONTENTS

LIST OF TABLES

LIST OF FIGURES

Chapter 1: The Titanium Contents of Lunar Mare Basalts

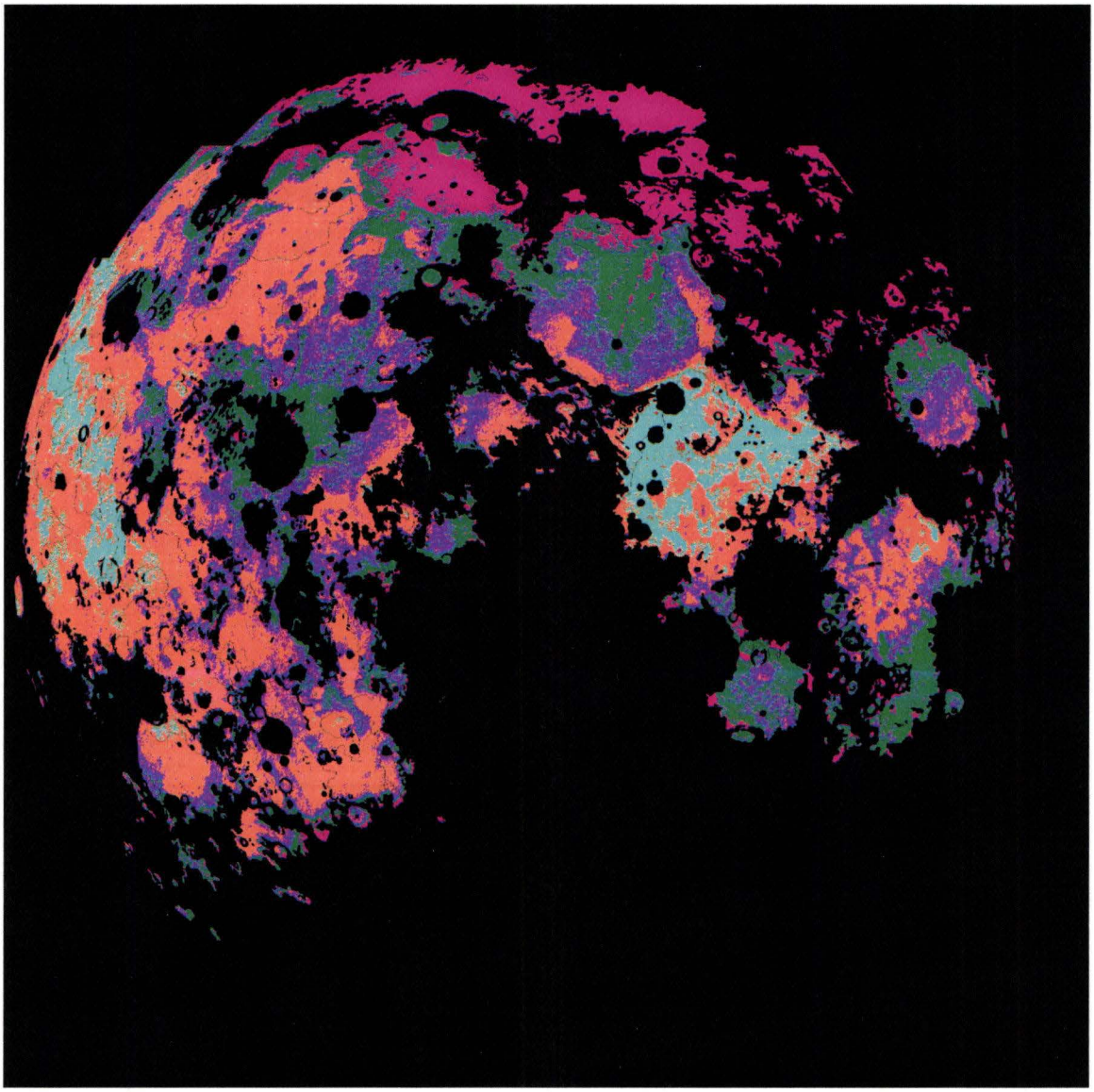

Titanium distribution of the lunar mare regions. TiO_2 content obtained from Galileo SSI image processed by the method of Lucey et al., 1996, 1998 and Blewett et al., 1997. Color coding (TiO2 wt. %): 0-1 magenta, 1-2 gray, 2-3 purple, 3-7 orange, and 7+ cyan. The TiO_2 divisions are selected to show detail in the low ranges where mare basalts are most spatially abundant. Very Low Ti basalts (VLT, <1.0 wt. % TiO_2) are primarily located in the northern/northeast mare. The lower range basalts (1.0-2.0 and 2.0-3.0 wt. % TiO_2) are widespread, occupying much of Mare Crisium, Mare Serenitatis, Mare Nectaris and sections of Mare Fecunditatis, Mare Imbrium, and areas of eastern Procellarum. The next higher basalt range (3.0-7.0 wt. % TiO_2) is found in western Mare Imbrium, northern Mare Fecunditatis, Mare Tranquillitatis and throughout Oceanus Procellarum. The higher Ti basalts (> 7.0 wt. % TiO_2) dominate Mare Tranquillitatis and Procellarum.

Mare basalts are classified largely on the basis of their TiO_2 contents, which varies in lunar samples from several tenths of a wt. % to about 13 wt. % (e.g., Taylor *et al.*, 1991 a; BVSP, 1981 a). The sample data suggest that there is a bimodal abundance of basalt types, divided into high-Ti and low-Ti basalts, with a distinct gap between them. The question is, does this distribution reflect the true nature of the mare basalts or is it due to the statistically small sample set that was obtained by the four Apollo and two Luna missions that landed in maria? While remote sensing data (e.g., Charette *et al.*, 1974; Head, 1976; Pieters, 1978) have provided some evidence for a continuum of mare Ti abundances, this has not been documented quantitatively. Our data (see below) demonstrate that there is a continuum of mare Ti contents, and that high-Ti mare basalts are not abundant on the lunar surface.

It is important to properly characterize lunar mare basalt compositions since they serve as probes of the interior composition of the Moon. To accurately use them to investigate the lunar interior, we need to know the full range of mare basalt compositions. The recent Galileo and Clementine missions allowed us to take a global look at the composition of the Moon. Previous comprehensive mapping efforts have estimated TiO_2 (Charette *et al.*, 1974; Head, 1976; Johnson *et al.*, 1977; Head *et al.*, 1978; Pieters, 1978; Metzger *et al.*, 1979; Davis, 1980; Jaumann, 1991; Johnson *et al.*, 1991; Greeley *et al.*, 1993; Pieters *et al.*, 1993; Melendrez *et al.*, 1994; Campbell *et al.*, 1997) and it has been suggested that relative FeO content can be estimated for a few cases from the depth of the 1.0 μm absorbtion band (Pieters, 1978). Recently,

analytical techniques for the accurate determination of FeO (Lucey *et al.*, 1995) and TiO_2 (Lucey *et al.*, 1996, 1998; Blewett *et al.*, 1997) abundances of lunar surface units from Clementine and Galileo spectral reflectance data have been developed. For this analysis, we applied the TiO_2 mapping technique to the Galileo data set acquired with the Solid State Imager (SSI) (Belton *et al.*, 1992) at a resolution of 1-2 km, and the Clementine (Nozette *et al.*, 1994) data set at resolutions of 125 m to 35 km.

Background

Previous studies have been made by the remote sensing community to extract quantitative geochemical information from Earth-based and spaced-based data for the Moon. The derived TiO_2 values from these studies have implied that mare Ti abundances vary continuously. The first successful derivation of elemental concentration was the mapping of Ti in mature mare soils via the correlation of the slope of the spectral curve between 0.402 and 0.564 μm and TiO_2 abundance (Charette *et al.*, 1974). This relationship was used to predict the Ti content of several unvisited mare surfaces. Subsequently, Head (1976) produced a generalized color difference map of the nearside lunar maria which showed intermediate values between the blue and red end members. The "Charette relation" was later used and improved upon by others, first by Johnson *et al.* (1977) and later by Pieters (1978) who used the relation to map and identify mare units of the lunar nearside. Two units called Medium (M, <4.0 wt. % TiO_2) and Medium High (MH, 3-7 wt. % TiO_2) by Pieters (1978) overlap the intermediate range (4.5-7.5 wt. % TiO_2) defined in this study. Johnson *et al.*

(1991) utilized CCD technology with improved photometric stability to produce a more accurate TiO_2 (±2 wt. %) abundance map for the entire lunar nearside maria. The preceeding studies used Earth-based spectral reflectance data for the Moon. The Galileo spacecraft SSI data allowed Pieters *et al.* (1993) to create a color composite mosaic which show mare materials with intermediate TiO_2 content. Other researchers have used a variety of remote sensing techniques to determine TiO_2 abundances on the Moon including: Apollo 15 and 16 gamma-ray spectroscopy (Metzer and Parker, 1979; Davis, 1980), Earth-based spectral reflectance (Jaumann, 1991; Melendrez *et al.*, 1994) , and Earth-based radar (Campbell *et al.*, 1997). The TiO_2 measurement techniques that utilize the Charette relation are limited to mature mare surfaces. Moreover, the technique exhibits large uncertainties for Ti contents below 3-4 % TiO_2 (Pieters, 1978, Johnson *et al.*, 1991) because Ti no longer UV-VIS spectral shapes of mare surfaces with these TiO_2 values. The analytical technique used in this paper accounts for FeO and maturity variations, and is applicable to Ti contents below 3 wt. %, thus allowing Ti-mapping to be extended to the lunar highlands and the low-Ti maria (Lucey *et al.*, 1995, 1996; Blewett *et al.*, 1997).

Methods

The TiO_2 values used in this study are derived from a technique using the Clementine and Galileo reflectance data (Lucey *et al.*, 1996, 1998). The technique was formulated using laboratory spectra and bulk chemical analysis of returned lunar soils. A plot of 0.415/0.750 μm vs. 0.750 μm reflectance for the Clementine (0.410/0.756 μm vs. 0.756 μm for Galileo) revealed trends related to

the abundance of opaque minerals in surface materials. Values of the UV ratio and reflectance for the Apollo and Luna landing sites were extracted from the Clementine 0.415 μm and 0.750 μm images and used to define a spectral parameter correlated to the average TiO_2 content of soils returned from each site (Blewett *et al.*, 1997). This technique is well calibrated in the 0.5 to 10 wt. % TiO_2 range, and is especially well calibrated above 2 wt. % (Lucey *et al.*, 1996). The standard deviation for all sites is ±1.14 wt % TiO_2, and will improve as the Clementine photometric calibration is refined (Blewett *et al.*, 1997). We used the resultant parameter to calculate the TiO_2 concentrations at each pixel from data acquired with the Solid State Imager during the second Earth-Moon encounter on Galileo and the UVVIS camera on Clementine. To isolate mare areas, we used a Geographic Information System (GIS) masking technique on a digital version of the lunar geologic map (Wilhelms and McCauley, 1971).

Results

Classification

Mare basalts are classified using several properties, including chemical composition, remanent magnetism, radioactivity, minerology, texture, and age (Soderblom *et al.*, 1977; Boyce, 1976; Boyce and Johnson, 1977). The chemical parameters commonly used to subdivide basalts are TiO_2, Al_2O_3, MgO, K_2O, and the Rare Earth Elements (REE). TiO_2 is especially useful as it exhibits the largest range of values, and provides a method of classification that is discernible using both chemical and remote sensing methods. Lunar sample workers commonly divide mare basalts into two main groups, low-Ti and high-Ti basalts

(e.g., Taylor *et al.*, 1991 b). They also recognize very-low-Ti basalts as those containing less than about 1.0 wt. % TiO_2 (e.g., Papike *et al.*, 1998). This basic dichotomy is apparent in Figure 1a where the samples are clustered as high and low Ti basalts. The sample data shows two peaks centered on 2.5-3.0 wt. % and 12-13 wt. %, with a distinct gap between ~6 - 9.5 wt. %. Basalts collected from the Apollo 11 and 17 sites generally have over 9.0 wt. % TiO_2 and samples collected at Apollo 12, 14, 15, and Luna 16 have less than about 6 wt. % TiO_2. The sample data in Figure 1a include rock samples, but not pristine lunar glasses. The rock samples which occupy the gap include the Apollo 14 mare basalt sample 1162 (clast DV-5) extracted from the polymict lunar breccia 14321 at 6.49 wt. % TiO_2 (Shervais *et al.*, 1985), the Apollo 17 sample 71095 with 7.7 wt. % TiO_2 (Neal *et al.*, 1990), and the Apollo 17 sample 71559 with 8.3 wt. % TiO_2 (Neal and Taylor, 1992). Most volcanic glasses also plot in low-Ti and high-Ti clusters, but two volcanic glass compositional groups (Apollo 17 yellow 6.90 wt. % TiO_2, Apollo 17 orange 8.63 wt. % TiO_2, Delano, 1986) have average TiO_2 abundances that fall in the sample gap.

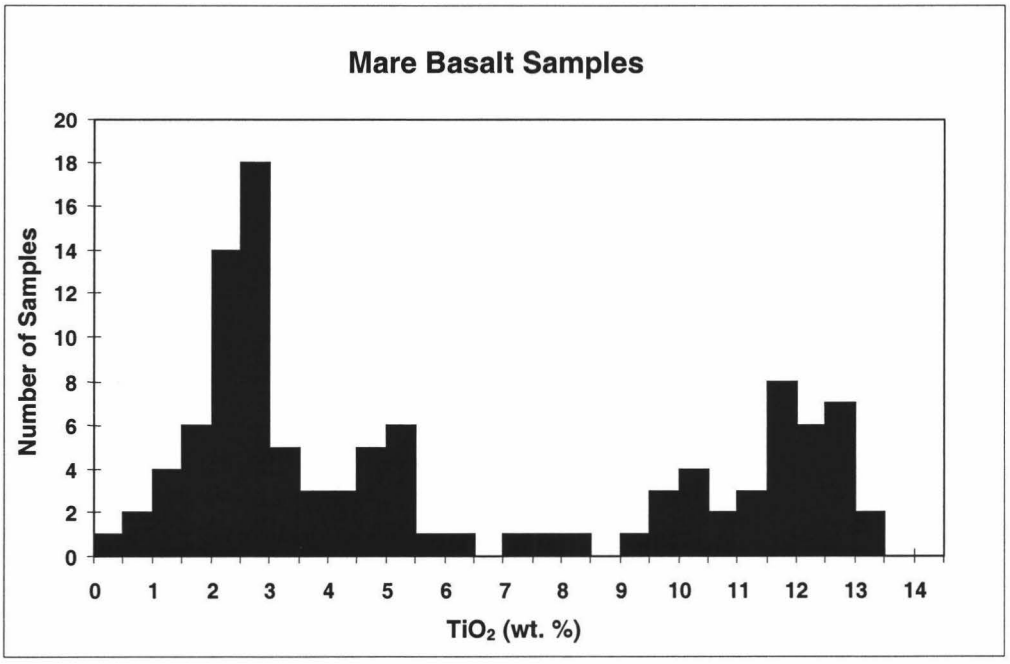

Figure 1a. TiO_2 distribution for the lunar maria constructed from sample data, excluding pyroclastic glasses. The histogram reveals a bimodal distribution of TiO_2 concentration.

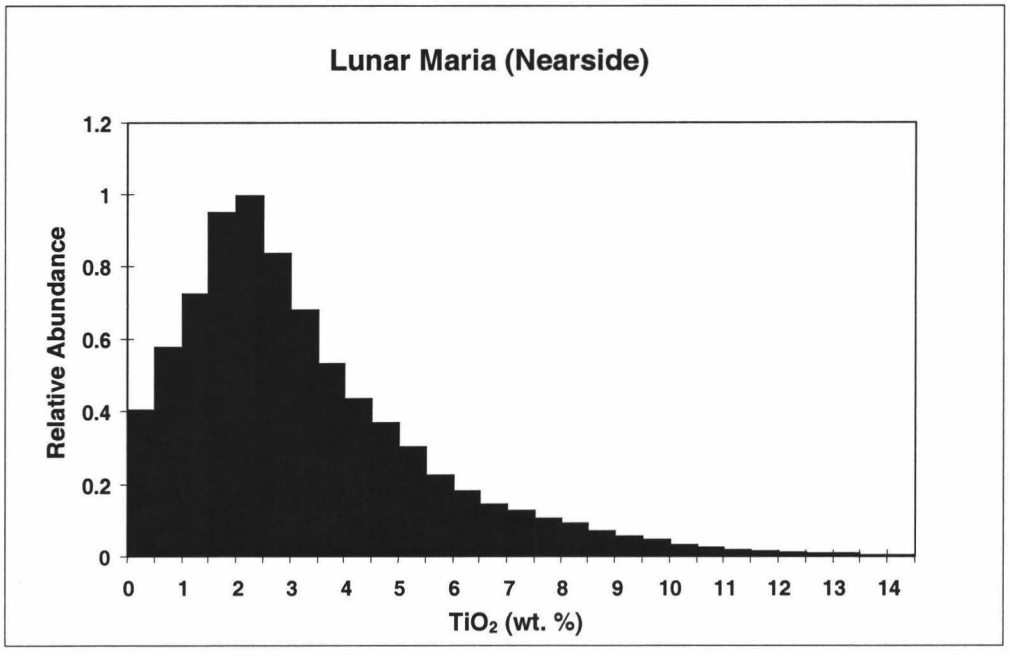

Figure 1b. Remotely sensed TiO_2 abundances for all nearside lunar mare. The TiO_2 distribution is continuous, with no hint of bimodality.

Investigators using remote sensing techniques use different classification schemes (Table 4). We suspect this is partly due to lower sensitivities at low-Ti contents of the Charette relation, and partly due to the difference between the compositions of mare basalt units and the regoliths that formed on their surfaces.

TABLE 1. Survey of TiO_2 Classifications

This Study (1999)		Melendrez *et al.* (1994)		Pieters *et al.* (1993)		Johnson *et al.* (1991)		Neal and Taylor (1992)		Davis (1980)		Johnson *et al.* (1977)		Papike *et al.* (1976)	
Remote		Remote		Remote		Remote		Sample		Remote		Remote		Sample	
Name	Range	Name	Range	Name	Range	Name	Range	Name	Range	Name	Range	Name	Range	Name	Range
Very Low	< 1.0		< 3.0	Low-TI	< 2.0		< 3.0	Very Low	< 1.0		< 0.5		< 2.0	Low-Ti	1.0 - 5.0
Low	1.0 - 4.5		3.0 - 6.0	Medium	< 4.0		3.0 - 4.0	Low	1.0 - 6.0		0.5 - 1.0		2.0 - 3.0	High-Ti	9.0 – 14.0
Inter-mediate	4.5 - 7.5		6.0 - 9.0	Med. High	3.0 - 7.0		4.0 - 5.0	High	> 6.0		1.0 - 1.7		3.0 - 6.0		
High	7.5 - 10.0		> 9.0	High-Ti	> 6.0		5.0 - 6.0				1.7 – 2.3		> 6.0		
Very High	> 10.0						6.0 - 7.0				2.3 – 3.0				
							7.0 - 8.0				3.0 – 4.0				
							8.0 - 9.0				4.0 – 5.8				
							9.0 - 10.0				> 5.8				
							> 10.0								

The relationship between basalts and the mare regoliths from which they were collected is shown in Table 5. The regolith samples collected from maria at the 11, 12, 15, and 17 Apollo sites have TiO_2 values that are lower than the basalt samples collected at the same site. The soil samples are diluted primarily with low-Ti highland material, and the resultant material has TiO_2 values 10 to 32% lower than the rock samples. Thus, if maria are classified by regolith TiO_2 content, the boundaries of the sample gap need to be shifted downwards by about 20% compared to a classification based on TiO_2 abundances in lunar samples.

TABLE 2. TiO_2 Values for Rocks and Regoliths*

Site:	Ap11	Ap12	Ap15	Ap17
Rocks:	10.4	3.62	2.0	11.9
Regolith:	7.94	2.61	1.8	8.1
%Diff:	-23.7	-27.9	-10.0	-31.9

* Data from Haskin and Warren (1991)

We have devised TiO_2 classification values which serves to illustrate this concept and highlight the unsampled areas of the Moon (Table 1). An "Intermediate" range (4.5-7.5 wt. % TiO_2) roughly corresponds to the mare basalt units that have not been sampled by any Apollo or Luna mission. This range corresponds to the gap in the samples (Figure 1a) when the sample TiO_2 values of 6 - 9.5 wt. % are adjusted downward by ~20 % to regolith TiO_2 levels. The remaining classifications used in this study include: "Very Low" as a commonly used designation for values below 1.0 wt. % TiO_2, "Low" for the range of 1.0-4.5

wt. % TiO_2, "High" for the range 7.5-10.0 wt. % TiO_2, and "Very High" for values greater that 10.0 wt. % TiO_2.

Global basalt inventory: not bimodal

Abundances derived from Clementine and Galileo multispectral data obtained for the lunar nearside indicate that the TiO_2 contents of the maria vary continuously from quite low values to high values, in contrast to our biased direct sampling of the Moon, which suggests a significant gap between low- and high-Ti basalts (Figure 1a). This is quantified in Figure 1b, which shows a histogram of the TiO_2 contents of nearside mare surfaces. The nearside image in Figure 2 shows the spatial distribution of the various basalt TiO_2 ranges. The mare units which cover the largest surface area contain 1-3.5 wt. % TiO_2 (Figure 1b), similar to basalts at Apollo 12, 14, and 15 (McKay *et al.*, 1991; Neal, 1999). Very-low Ti basalt units (VLT) are less common, but significant. VLTs occur in the northern portions of Mare Serenitatis, Mare Crisium, and Mare Imbrium. They extend north of these maria to Mare Frigoris, which is composed predominately of VLT basalts. The abundance of mare basalts decreases as TiO_2 increases from the peak between 1 and 3.5 wt. %. The intermediate basalts (4.5-7.5 wt. % TiO_2) are primarily found within Mare Tranquillitatis, the western side of Mare Imbrium, and much of Oceanus Procellarum. Small areas are located in northeastern Mare Fecunditatis and the northern part of Mare Humorum, and minor amounts are located throughout maria on the central nearside. Only 10 % of mare surfaces exhibit > 6 wt. % TiO_2, and only 5% of the mare surface contain >7.5

wt. %. These correspond to mare basalt samples with TiO_2 contents of ~7.5 wt. % and 9 wt. %, respectively. Mare units that exhibit high and very high TiO_2 abundances are confined mainly to Mare Tranquillitatis and Oceanus Procellarum.

The TiO_2 values in Figure 2 were derived from data obtained with the Galileo SSI instrument, and are confined to the nearside only. A parallel analysis was performed on the TiO_2 distribution of the farside maria using Clementine multispectral imagery with spatial resolution of 35 km. The results showed that these farside maria are dominated by very-low Ti surfaces (< 1.0 wt. %) and exhibit lesser expanses of low Ti (1.0-4.5 wt. % TiO_2) material. These findings are supported by higher resolution (250 meter/pixel) Ti mapping of far side basalts (Gillis and Spudis, 1998). The low-Ti nature of these basalts combined with the small areal extent (15% of the mare surfaces) would not alter the histogram (Figure 1b) significantly.

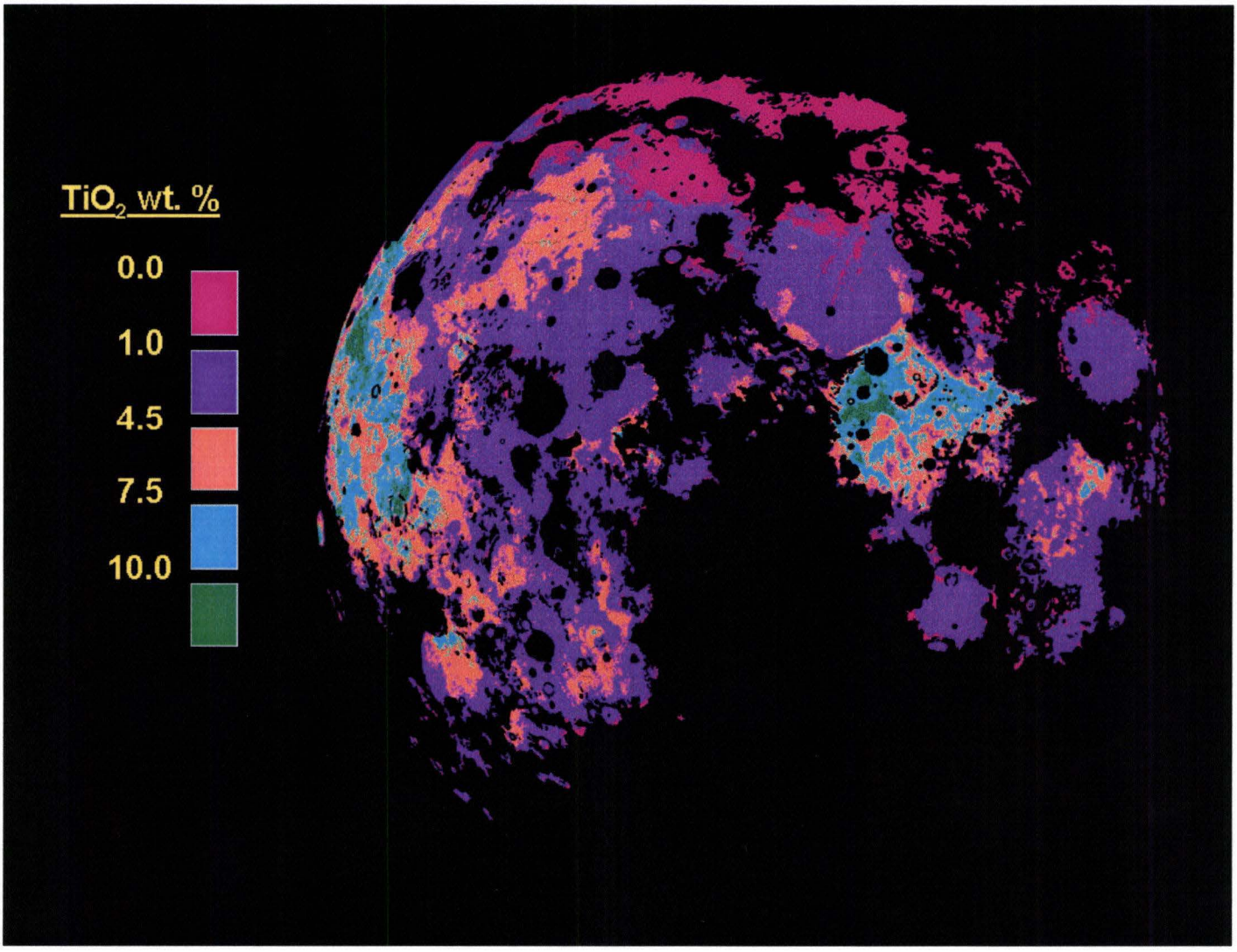

Figure 2. Galileo SSI nearside image (resolution 1 – 2 km) which shows only mare regions; all other geologic units have been masked. The TiO_2 distribution shown in the histogram (Figure 1b) is apparent in the image; Very Low (< 1.0 Wt. % TiO_2) and Low (1.0-4.5 wt. % TiO_2) dominate much of the mare surface area. Intermediate (4.5-7.5 wt. % TiO_2) mare basalts are colored orange, and located in portions of Mare Tranquillitatis, parts of the western side of Mare Imbrium, and in large portions of Oceanus Procellarum. Small areas of Intermediate mare basalts are also located in northeast Fecunditatis and the north end of Mare Humorum, as well as other locations. High TiO_2 values are exhibited by mare deposits in portions of Mare Tranquillitatis and Oceanus Procellarum.

The relationship between the Apollo and Luna landing sites and the intermediate (4.5-7.5 wt. %) TiO_2 mare units is shown in Figure 3. The gap in the sample data (6.0-9.5 wt. %) in Figure 1a roughly corresponds to these intermediate mare unit values when adjusted downward to take into account contamination of regoliths with highlands debris. The Apollo sites were not in close proximity to the intermediate Ti basalts, and of the three Luna missions only Luna 16 falls near an intermediate basalt boundary. The TiO_2 content in Luna 16 sample 21013,8 is 5.1 wt. % (Ma *et al.*, 1979), which is still below the lower end of the intermediate range and the average Luna 16 regolith sample contains only 3.3 wt. % TiO_2 (Haskin and Warren, 1991), firmly in the low-Ti range. Clementine high resolution images concur that the Luna 16 site contains about 3.0-3.5 wt. % TiO_2 (Blewett *et al.*, 1997).

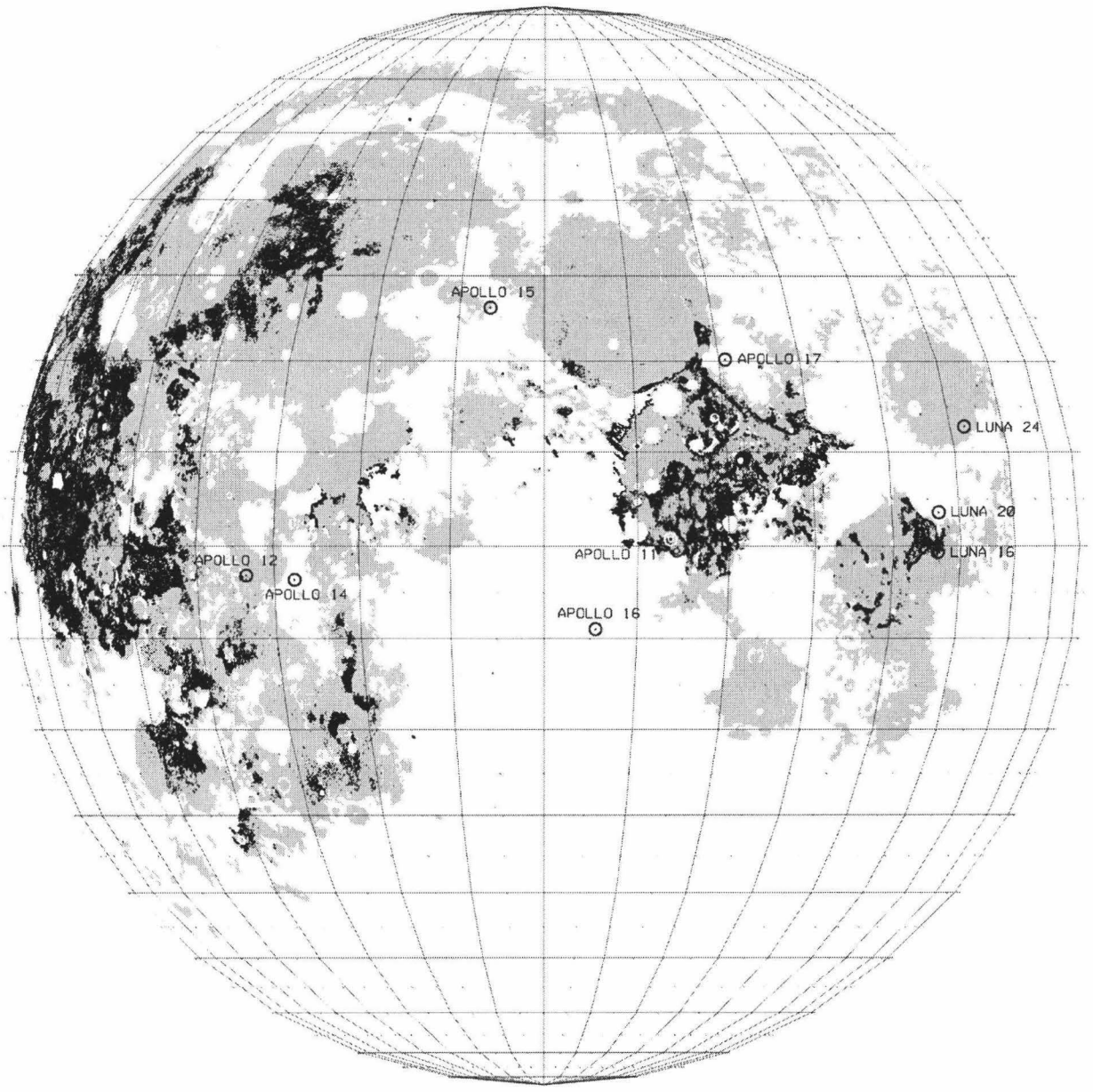

Figure 3. Apollo and Luna landing sites are shown in relation to the Intermediate mare basalts (4.5-7.5 wt. % TiO_2), which are the black regions. Low and high-Ti areas are gray; highlands are white. The landing sites fall outside of the intermediate mare regions.

Discussion

Mare basalts were produced by melting of an olivine and pyroxene mantle and as such, provide information about the interior of the Moon. If the melting process involved chemical equilibrium between the melted and unmelted portions, then the lavas will preserve clues to the chemical and mineral compositions of the regions that underwent partial melting. Mare basalts preserve evidence of the lunar magma ocean in the form of depleted europium and alumina and enriched iron concentrations consensually attributed to the sinking of olivine and orthopyroxene phases and the complementary floatation of plagioclase (Taylor, 1982; Ryder, 1991). The large range in Ti contents of mare basalts suggests a diversity of mantle compositions or complex mantle dynamics, or both.

One might argue that mare units (Figure 2) that exhibit intermediate TiO_2 contents of 4.5-7.5 wt. % are not the product of a source region with intermediate composition, but instead are created by other processes such as the impact mixing of high-Ti and low-Ti mare basalts that overlie one another or by vertical or horizontal mixing of high-Ti basalts and low-Ti highlands material. This is possible in some cases, as lateral mixing may be the explanation for the thin line of intermediate basalts, adjacent to highlands material, along the northeast edge of Mare Tranquillitatis. However, it seems unlikely that such mixing is so efficient that it can account for the paucity of high-Ti basalts. Several areas of the Moon illustrate the distinctness of mare basalts. The boundary between the low-Ti basaltic deposits of Mare Serenitatis and the higher-Ti units of Mare

Tranquillitatis is very distinct (e.g., Melendrez *et al.*, 1994; Bell and Hawke, 1995). Figure 4 shows a portion of this boundary and demonstrates the lack of mixing between the low-Ti basalts of Mare Serenitatis and the higher-Ti intermediate unit which it embays. Mixing has an effect over short distances, with the most extensive mixing occurring within 2 km of the contact and less mixing occurring within 10 km of the contact (Mustard *et al.*, 1998). (Small fresh craters appear dark in Figure 4 since the algorithm used to generate the image is optimized for TiO_2 and not for maturity.) The intermediate Ti basalt deposit is minimally contaminated by the adjacent low-Ti material, lowering the TiO_2 content by about 1.5 wt. %. Despite the reduction in TiO_2 content for the higher TiO_2 unit, there is more than a 3.0 wt. % difference between the two units. A comparison of the distinctive characteristics of the two mare units is listed in Table 3.

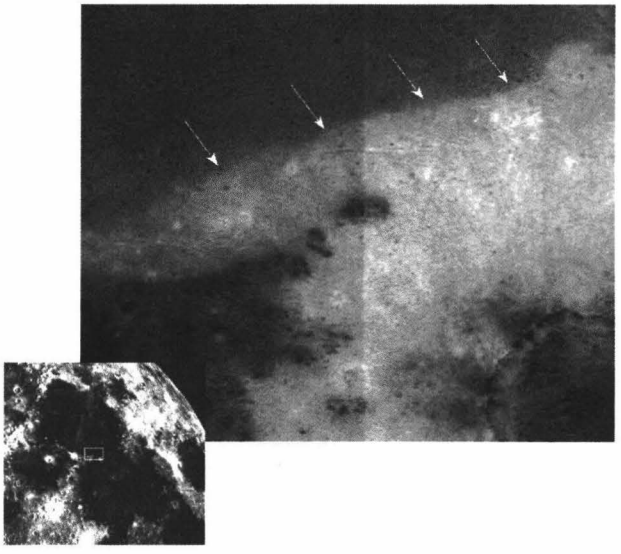

Figure 4. Clementine medium-resolution (0.5 km) TiO_2 image of the Mare Serenitatis/Mare Tranquillitatis boundary (arrowed). The location of this image is outlined in white on the inset. The relatively higher-Ti (6.0+ wt. % TiO_2)basalts from Mare Tranquillitatis appear to be distinct from the lower-Ti (3.0 wt. % TiO_2) basalts for Mare Serenitatis, reflecting distinct magma and mantle source compositions.

TABLE 3. Comparison of Mare Units in southeast Serenitatis (reference Fig. 4)

Location	Age (Boyce, 1976)	Spectral Class (Pieters, 1978; BVSP, 1981 b)	Structural Features (Wilhelms, 1987)	TiO_2 wt. % (Melendrez *et al.*, 1994)
Northern Unit	D_L=241-260 m 3.4 ± 0.1 b.y.	hDWA	Unfaulted	3.0
Southern Unit	D_L=311-380 m 3.75 ± 0.05 b.y.	HDWA	Faulted by conspicuous arcuate grabens	6.0

The lava flows on the west side of the Imbrium basin are not extensively mixed, have distinctive morphology, and are composed of intermediate TiO_2 basalts. These Eratosthenian age deposits are thought to have originated from a single eruptive source region in the south-southwest corner of the basin. There may have been three major eruptive periods between 2.5 and 3.0 ba which extended between 400 and 1200 km. Three geochemical provinces have been identified in an area north of crater Euler (Friedman et al., 1996). The morphology of the flows show little erosion and are well preserved due to their young age. Flow lobes, leveed flow channels, and scarps up to 60 m high are distinctly visible (Schaber, 1973). The relatively pristine nature of the flow structures is one indication that the area has not been heavily disturbed by impact events. A visual inspection of the Imbrium region in Figures 2 and 3 shows that the flow areas are predominately composed of intermediate TiO_2 basalts and are fairly uniform. A histogram of the northern portion of the Imbrium flows (Figure 5) provides some insight into their composition. The bulk of the distribution falls within the 4.5-7.5 wt. % intermediate boundary. The shape of the histogram is significant as it is apparent that the low end of the distribution rises gently, whereas the high end of the distribution drops off abrubtly. The shallow rise on the low end is a sign that the intermediate basalts have been mixed with either low-Ti basalts or highlands material, although the TiO_2 range of the rise suggests the former is more likely. This mixing tends to draw the distribution toward the low-Ti end of the histogram. The high-Ti end of the histogram falls off sharply which indicates that there has been little alteration

from low-Ti. In some areas, apparently intermediate basalts may have been created by combining low-Ti and high-Ti material to arrive at an average between the two end members. This is not the case in the Imbrium flows, as there are no high-Ti basalts in either the low resolution (1-2 km/pixel) Galileo images, nor the high resolution (125 m/pixel) Clementine images. If high-Ti basalts existed in the young Imbrium flows there would be remnants still visible, but Figure 5 shows that there are virtually no basalt units with 8 wt. % TiO_2 or above.

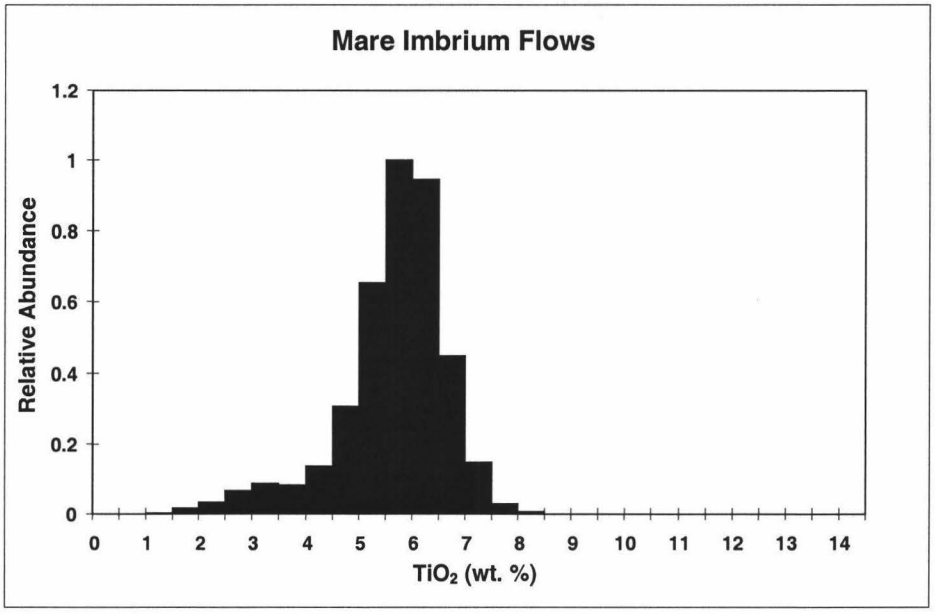

Figure 5. Remotely sensed TiO_2 abundances for the northern half of basalt flows on the west side of Mare Imbrium. The TiO_2 distribution indicates that the flows in this region are composed of intermediate mare basalts (4.5-7.5 wt. % TiO_2).

We conclude that low-Ti mare basalts are the most spatially abundant. The mixing of these basalts with higher-Ti basalts tends to dilute the TiO_2 values, creating lower average TiO_2 values overall. However, there are clear cases where the basalt units are distinctly intermediate in composition and the mixing is a secondary effect.

The surface distribution of basalt Ti contents may be due to a variety of factors. These include the Ti content of the lunar mantle, the ease of melting of mantle sources with various Ti contents, and the efficacy of magma transport in the mantle. Mantle sources with the lowest solidi and highest concentrations of radioactive elements would be most prone to melt. Such sources could form late in the crystallization of the lunar magma ocean, when incompatible elements such as U, Th, and K were enriched and temperatures were lower. These sources would also be richest in TiO_2. This suggests that high-Ti basalts ought to be more abundant than lower-Ti varieties because the high-Ti source regions melted easier. On the other hand, high-Ti basalt magmas have higher densities, which inhibits their migration through the low-density crust, leading to more intrusions and fewer eruptions of high-Ti mare magmas than of other types. So, high-Ti magmas might form more easily because they melt at lower temperatures than other mare basalts source regions, but their migration to the surface is more sluggish than lower-Ti basalts. We assume that these effects balance each other and that the distribution of mare basalt Ti contents reflects the variation in the Ti concentrations throughout the mantle. The lunar far side may be an exception. Robinson *et al.* (1992) and Gillis and Spudis (1998) suggest that the lack of very high-Ti basalts found on the eastern limb and far side could be caused by a thicker crust filtering higher density VHT basalts (Delano, 1990). This would indicate that buoyancy is a major factor when the crustal thickness exceeds approximately 50 km.

Taken at face value, the distribution of the TiO_2 contents of mare deposits shown in Figure 2 is consistent with models of the formation of their source regions as cumulates from the lunar magma ocean (e.g., Taylor and Jakes, 1974; Taylor, 1982; Warren, 1985), coupled with dynamic mixing of sinking, dense, Ti-rich and Fe-rich late-stage cumulates and rising Mg-rich early cumulates or undifferentiated rock (Dowty , 1975; Kesson and Ringwood, 1976; Herbert, 1980; Ryder, 1991; Hess , 1991; Hess and Parmentier, 1995). Figure 6 shows a model of the lunar interior with cumulate source regions produced in the magma ocean, assuming simple fractional crystallization.

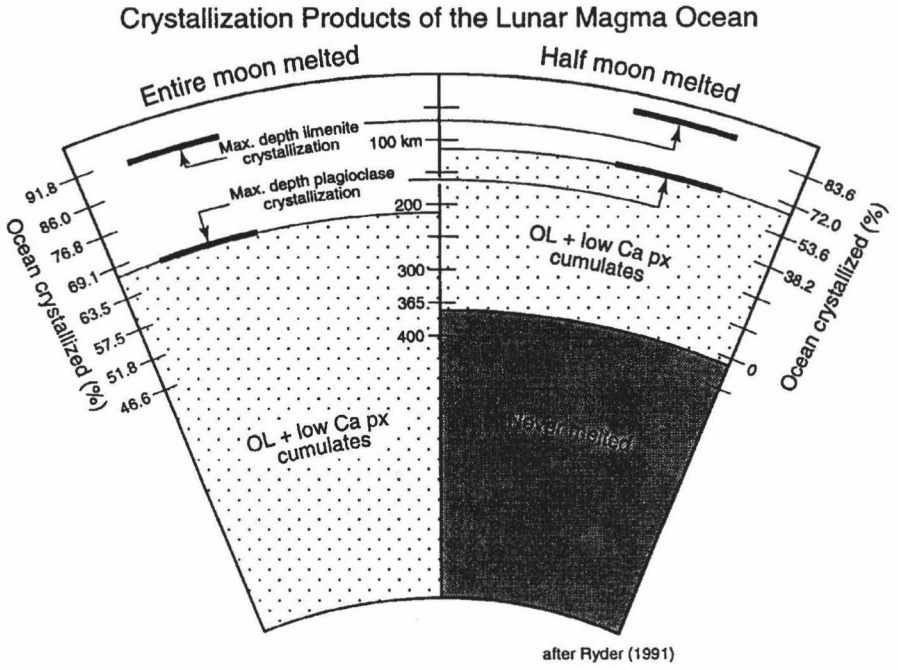

Figure 6. Two scenarios for the crystallization of the lunar magma ocean as presented by Ryder (1991). In both the whole-Moon melting and half-Moon melting cases, cumulates dominated by olivine and orthopyroxene, which could melt to produce low-Ti basalts, constitute almost 70% of the crystallized magma ocean. In contrast, the ilmenite-bearing sources that produced high-Ti basalts constitute only about 10% of the cumulate pile. Mixing ilmenite-bearing rocks with Ti-poor early cumulates would produce intermediate-Ti basalts.

The mare basalts with <~5 wt. % TiO_2 formed by partial melting of olivine and orthopyroxene cumulates with low abundances of TiO_2, like those produced experimentally (Longhi, 1992). Such cumulates would have been the most abundant product by far of the lunar magma ocean, accounting for at least 70 vol. % of the cumulate pile (e.g. Taylor and Jakes, 1974). Thus, the fact that 80% of the mare basalts contain < 5 wt. % TiO_2 is consistent with their origin as partial melts from cumulates formed in the lunar magma ocean. Formation of mare basalts with >5 wt. % could have involved dynamic mixing of these early cumulates with late-stage cumulates rich in clinopyroxene and ilmenite (Dowty, 1975; Herbert, 1980; Ryder, 1991; Hess, 1991; Hess and Parmentier, 1995; Lucey *et al.*, 1996). Ilmenite-bearing cumulates would make up 5-10 vol. % of the cumulate pile because ilmenite would not have reached saturation in the residual liquid until >90% of the magma ocean had solidified (Figure 6), thus accounting for the rarity of high-Ti mare basalts. The extent to which a hybrid source contained the ilmenite-rich cumulates was a major factor in determining the final TiO_2 content of the mare basalt magma produced. This model predicts that basalts with intermediate TiO_2 contents ought to be more abundant than those with high-Ti, in accord with our observations (Figure 1b). It is likely that even the low-Ti basalts (1.0-4.5 wt. % TiO_2) formed from hybrid sources, though with much less ilmenite; otherwise, it is difficult to explain their high Mg/Fe ratios and europium anomalies (Ryder, 1991).

Conclusions

The classification of lunar samples based on TiO_2 contents suggests that the distribution of mare basalts is bimodal, with a distinct gap between the high-Ti and low-Ti basalts. The global inventory of mare basalts shows that TiO_2 abundances vary continuously, not bimodally. Low-Ti (1.0 – 4.5 wt. % TiO_2) maria are most abundant, with the abundance decreasing as TiO_2 increases. High-Ti (>7.5 wt. % TiO_2) maria constitute only 5 % of the lunar maria. The lunar sample collection is clearly a biased sampling of the lunar maria. The landing sites are not located in regions of intermediate (4.5 – 7.5 wt. %) TiO_2 content.

This distribution of basalt compositions is consistent with formation of mare basalt mantle source regions from a lunar magma ocean. Although some of the intermediate basalts may be the result of impact mixing of high-Ti material with low-Ti material, this is not true for most intermediate areas. Magma ocean models predict a small abundance of ilmenite-rich cumulates (which would produce high-Ti basalts), in accord with our observation. The higher abundance of intermediate basalts (4.5 – 7.5 wt. % TiO_2) compared to high-Ti basalts emphasizes the importance of dynamic mixing of source regions during the evolution of the lunar mantle and the production of mare basalt magma.

Chapter 2: Igneous activity in the southern highlands of the Moon

Prior to the Apollo missions, the nature and origin of lunar dark-haloed and dark-rayed craters were the sources of much controversy. Most lunar scientists supported a volcanic origin for these features, but some advocated formation by impact processes [*e.g.*, *Shoemaker and Hackman*, 1962; *Wilhelms and McCauley*, 1971; *Scott*, 1972; *Head and Wilson*, 1979]. During the Apollo 17 mission, the astronauts actually visited and sampled the dark-haloed Shorty crater, which proved to be of impact origin [*Wilhelms*, 1987]. As a result of sample, geologic, and remote sensing studies in the immediate post-Apollo era, our understanding of lunar impact and volcanic processes was greatly increased and a number of investigators developed criteria for determining the origin of dark-haloed crater (DHCs) [*Schultz and Spudis*, 1979, 1983; *Head and Wilson*, 1979; *Hawke and Bell*, 1981]. Some DHCs were found to be of endogenic origin. These volcanic features were the source vents for the surrounding dark, localized pyroclastic deposits emplaced by vulcanian-style explosive eruptions [*Head and Wilson*, 1979; *Hawke et al.*, 1989; *Gaddis et al.*, 2000]. A much larger number of DHCs are of exogenic origin. Most of these impact craters exhibit dark ejecta deposits because they have excavated buried mafic units [*Schultz and Spudis*, 1979, 1983; *Hawke and Bell*, 1981]. These mafic units are most commonly buried mare basalt flows, but in some instances, may be intrusions (i.e. dikes, sills, etc.) of basaltic composition. Some exogenic DHCs were formed by the emplacement of a dark glassy veneer of impact melt near the crater rim crest [*Hawke and Head*, 1977; *Schultz and Spudis*, 1979]. Numerous studies have

demonstrated that detailed investigations of both endogenic and exogenic DHCs can provide critical information concerning the geology, composition, and evolution of selected portions of the lunar surface [*Schultz and Spudis*, 1979, 1983; *Hawke and Spudis*, 1980; *Hawke et al.*, 1985, 1989; *Blewett et al.*, 1995; *Antonenko et al.*, 1995; *Gaddis et al.*, 2000].

Several dark-haloed and dark-rayed craters have been identified in the Maurolycus region of the lunar nearside [*Shoemaker and Hackman*, 1962; *Scott*, 1972; *Giguere et al.*, 1998, 2000; *Hawke et al.*, 1998, 1999]. The Maurolycus region (Figures 7 and 8) is located in the southeastern highlands and includes densely to moderately cratered terrain with many craters larger than 45 km in diameter. *Scott* (1972) noted that the major stratigraphic units included the pre-Imbrium aged Janssen Formation, hummocky terra and pitted plains materials, and extensive clusters of bowl-shaped craters. The purposes of this study are to determine the composition and origin of DHCs in the Maurolycus region and to assess the implications for intrusive and extrusive igneous activity in the southern highlands of the Moon.

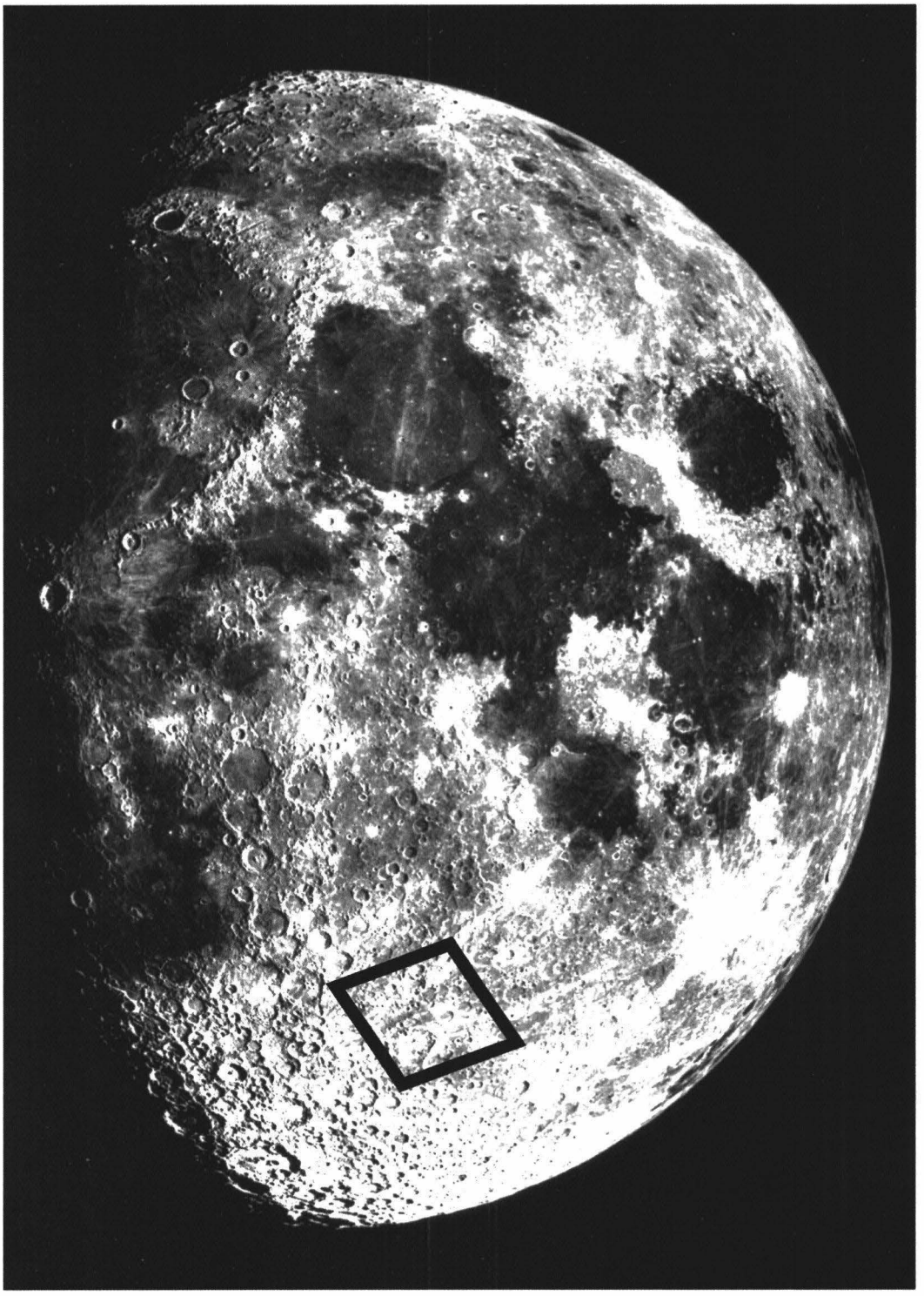

Figure 7. The lunar nearside. The box in the southeastern highlands identifies the study area and is shown in Figure 8. Lick Observatory photograph.

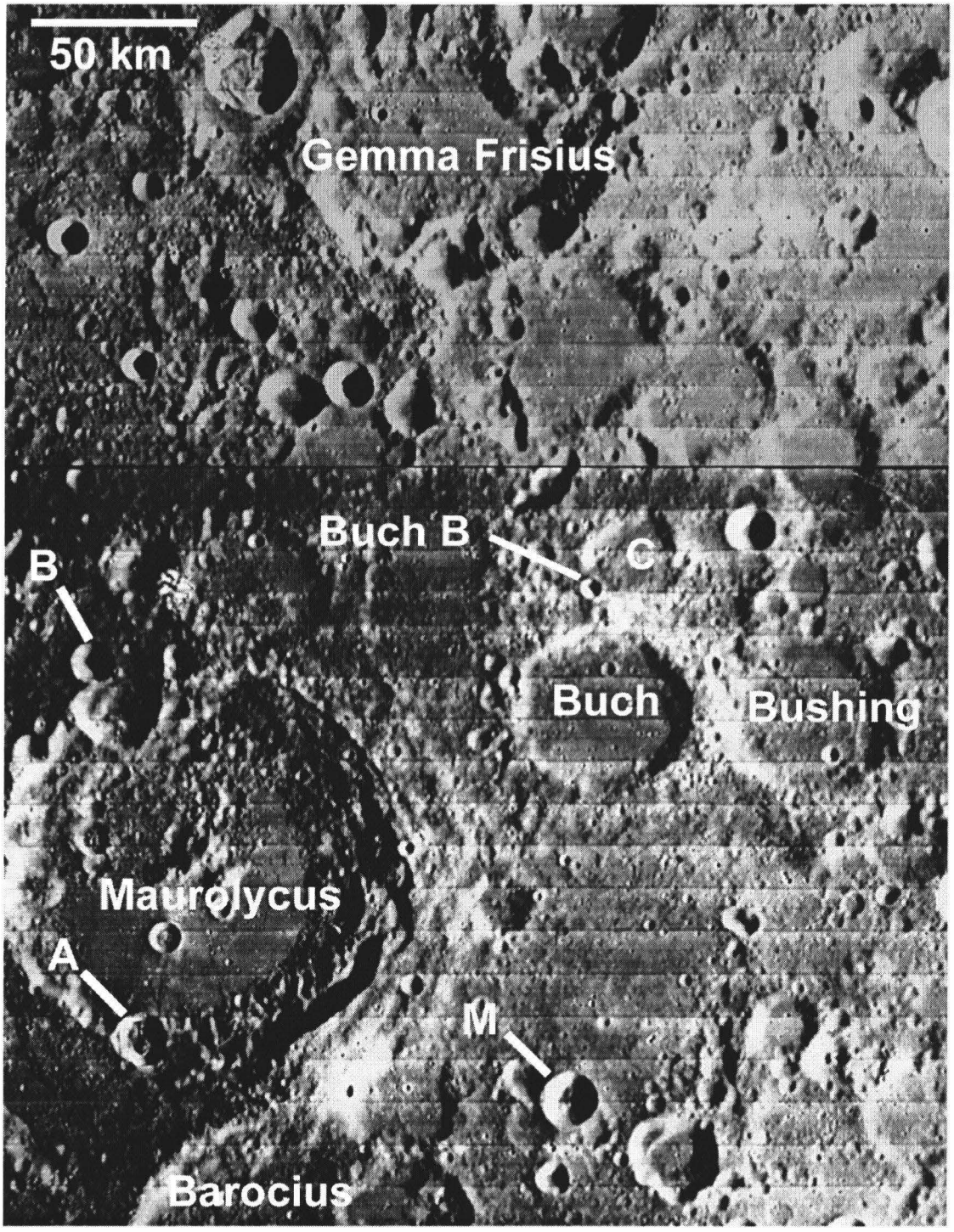

Figure 8. Area around Maurolycus crater (114 km diameter) which is located at 14.0° E, 41.8° S. The crater Buch B (6 km diameter) is located to the northeast at 17.0° E, 39.9° S. The craters mentioned in the text (Barocius M, Maurolycus A and B, and Buch B) are identified. Lunar orbiter IV images 95-2 and 95-3.

Methods

A wide variety of remote sensing and photographic data was utilized to investigate volcanic processes in the Maurolycus region. The lunar imagery included Earth-based telescopic photographs, Lunar Orbiter IV and V photographs, and Clementine images.

Both Galileo SSI [*Belton et al.*, 1992] and Clementine UV-VIS [*Nozette et al.*, 1994] images were used in this study. The most recent calibrations of each data set were utilized to produce FeO, TiO_2, and optical maturity maps of the Maurolycus region with a variety of spatial resolutions (35 km/pixel, 1 km/pixel, 125 m/pixel). The methods described by *Lucey et al.* [1995, 1998, 2000a, 2000b] and *Blewett et al.* [1997] were used to produce these composition and maturity images.

The 3.8 cm radar images of *Zisk* [1974] were utilized to investigate particle size distribution in the near-surface environment. Finally, the thermal data of *Shorthill and Saari* [1969] were used to study thermal anomalies in the Maurolycus region.

Results and Discussion

The most striking albedo anomaly in the Maurolycus region is associated with Buch B crater. This circular feature (diameter = 6 km) is located at 17.0° E, 39.9° S and is centered near the southern rim crest of Buch C crater (Figure 8). The crater exhibits a dark halo and dark rays (Figure 9a). However, some portions of the exterior deposits are relatively bright. *Shoemaker and Hackman* [1962] first described this unusual feature and suggested that it was the product

of relatively recent volcanic activity. Buch B was mapped by *Scott* [1972]. He noted the dark rays appear to interrupt bright Tycho rays and that the apparent superpositions of dark rays on Tycho rays, as well as a high infrared thermal anomaly, indicated a late Copernican age. *Scott* [1972] interpreted Buch B as possibly volcanic in origin and noted that the dark rays may be new volcanic material from an explosive maar-type vent.

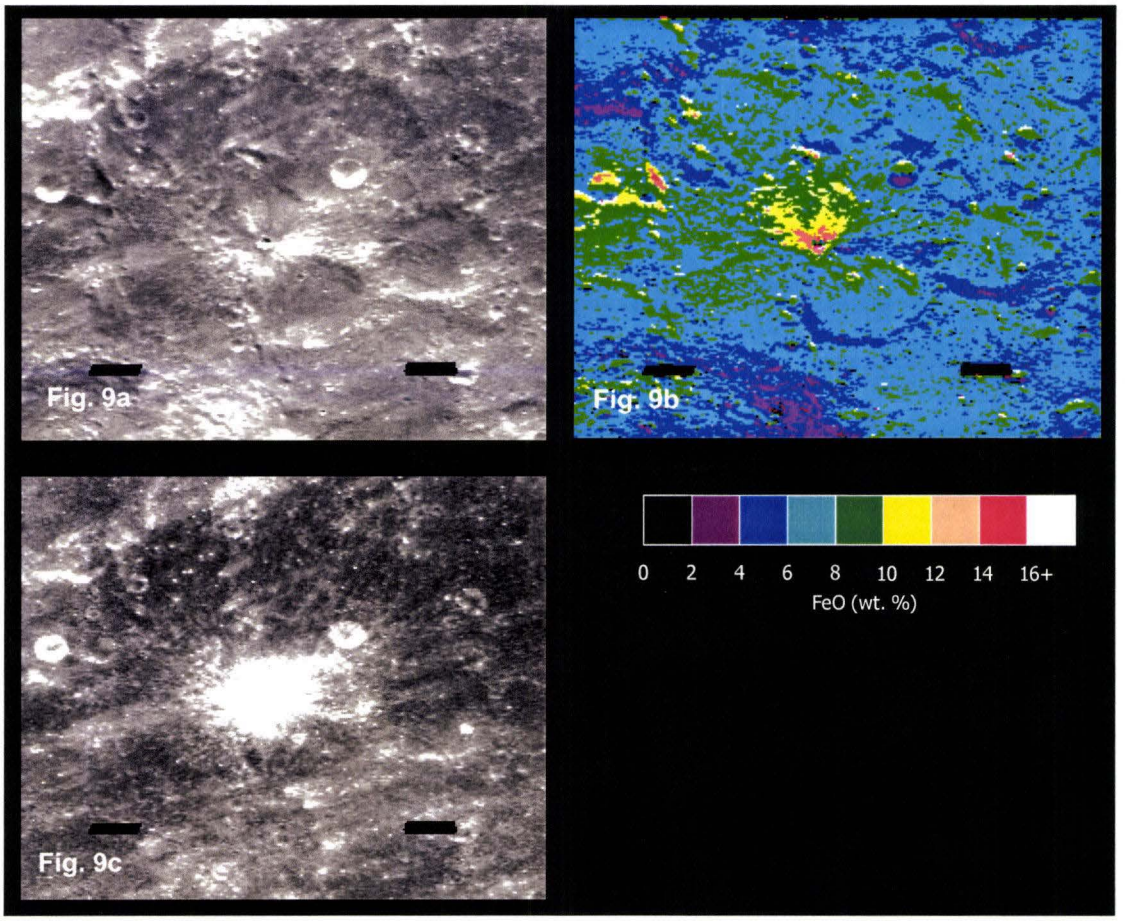

Figure 9a. Albedo image of crater Buch B (0.75 μm) from Clementine image (1 km/pixel). The dark halo surrounding the crater is apparent. **Figure 9b.** FeO image of crater Buch B derived from Clementine image (1 km/pixel). Images from method of Lucey and Blewett [2000b]. **Figure 9c.** Optical maturity image of crater Buch B derived from Clementine image (1 km/pixel). Images from method of Lucey *et al.* [2000a]. Maturity scale: immature areas are bright and mature areas are dark.

As discussed above, firm criteria for determining the origin of lunar craters were developed and tested in the post-Apollo era [*e.g.*, *Schultz and Spudis*,

1979, 1983; *Head and Wilson*, 1979]. Application of these criteria to Buch B leaves little doubt that it was formed by impact processes. For example, Buch B has a well-defined raised rim and a depth/diameter ratio typical of fresh impact craters. The crater is circular, not elongate in shape and there is no obvious association with well-developed faults or fractures. Buch B is clearly a dark-haloed impact crater, not a volcanic vent.

A major effort was made to determine the composition and origin of the dark ejecta associated with Buch B crater. Previous studies have demonstrated that some very young impact craters exhibit low-albedo exterior deposits composed of dark, glassy impact melt [*Hawke and Head*, 1977; *Schultz and Spudis*, 1979]. For craters less than ten kilometers in diameter, these exterior impact melts typically occur as a narrow fringe of glassy veneer immediately adjacent to the rim crest. The Buch B dark exterior deposits exhibit none of the characteristics of glassy impact melt deposits associated with craters in this size range.

The absence of glassy melt is confirmed by the optical maturity image (Figure 9c). The net effect of glassy impact melt on spectral properties is to lower the albedo and to reduce the depth of the one-micron absorption feature [*Hawke et al.*, 1979; *Smrekar and Pieters*, 1985]. These spectral changes would be reflected in the maturity image as areas of greater optical maturity [*Lucey et al.*, 2000a]. No abnormally mature areas can be seen in Figure 9c. Hence, impact melt plays no role in producing the dark halo and rays associated with Buch B.

Additional evidence for the composition and origin of the Buch B dark ejecta is provided by the 0.75 μm albedo image and the FeO map (Figures 9a and 9b). There is a good correlation between low-albedo exterior deposits and areas with high FeO values (12 – 14 %). These values approach those exhibited by lunar mare basalt deposits (15 – 18 %) [*Lucey et al.*, 1995]. In contrast, typical highland material in the Maurolycus region have FeO abundances that range between 5 and 9 %. The darkest portions of the exterior deposits appear to be composed almost exclusively of basaltic material. The higher-albedo ejecta deposits exhibit a range of FeO values (5 – 11 %). The lower values are consistent with the presence of local highland material while the higher values suggest a mixture of local highland debris with minor amount of basaltic material.

Additional support for the dominance of mare basalt in the dark exterior deposits of Buch B is provided by the TiO_2 map of the Maurolycus region. The highland terrain in the region exhibits TiO_2 values of less than 1 %. In contrast, portions of the Buch B dark ejecta have TiO_2 values between 1 % and 2 %.

In order to further investigate the composition of Buch B ejecta, five point spectra were extracted from calibrated and registered Clementine UV-VIS images [*Robinson et al.*, 1999; *Isbell et al.*, 1999; *Eliason et al.*, 1999] using the techniques described by *Tompkins and Pieters* [1999]. Spectra were obtained for the ejecta deposits associated with fresh impact craters in the southern highlands. These craters generally expose material dominated by noritic anorthosite or anorthositic norite. The two fresh highland spectra shown in Figure 10 were obtained for immature noritic anorthosite lithologies. Two typical

spectra for the exterior deposits of relatively young impact craters in mare regions are shown in Figure 10. These spectra exhibit strong "1 μm" absorption features and the band shapes indicate mafic assemblages dominated by high-Ca clinopyroxene.

Spectra were extracted for different portions of the Buch B dark exterior deposits including the dark ray that extends northwest from the parent crater. Two of these spectra are shown in Figure 10. These spectra have relatively strong "1 μm" absorption bands and have band parameters that suggest the dominance of high-Ca pyroxene. The spectra are very similar to those collected for fresh mare craters and the dark ray segments for which the spectra were obtained are composed of very immature mare basalt or immature mare basalt contaminated with minor amounts of highland debris.

Spectra were also obtained various portions of the bright Buch B ejecta deposits. Two of these spectra are shown in Figure 10. Although the areas for which these spectra were extracted are dominated by fresh highland material, some have spectral characteristics that suggest that small amounts of mare basalt may be present.

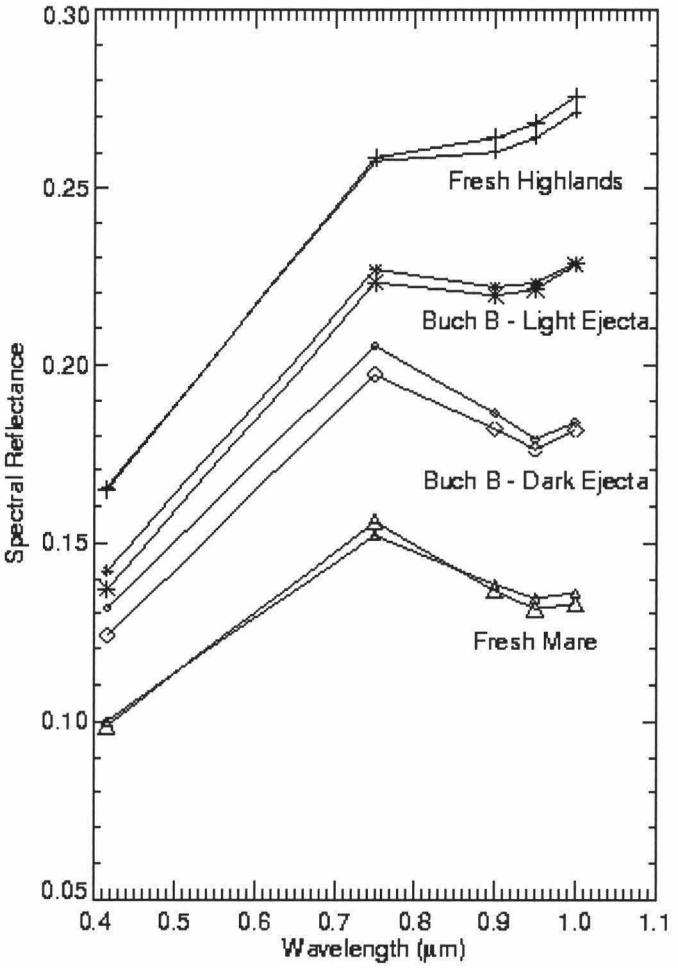

Figure 10. Five point spectra of Buch B and surrounding area were obtained from Clementine UV-VIS images with method of Tompkins and Pieters [1999]. Pairs of spectra were collected for four areas: fresh highland (plus), Buch B light-colored ejecta (star), Buch B dark-colored ejecta (diamond), and fresh mare (triangle).

Infrared thermal anomalies of the eclipsed Moon are believed to be related to the thermal conductivity of lunar surface material [*Shorthill and Saari*, 1969]. High values are generally thought to be related to the surface exposure of fresh rocks. *Scott* [1972] noted that the temperature of Buch B was about 22 K higher than its surroundings and suggested that Buch B was the youngest clearly visible Copernican crater in the region. The crater also exhibits enhanced returns in the

depolarized 3.8 cm radar images presented by *Zisk* [1974]. This radar anomaly indicates a high abundance of 1-50 cm fragments at or near the surface.

In summary, Buch B is a very young Copernican-age impact crater surrounded by both light and dark ejecta deposits that exhibit a high abundance of immature rock fragments. The dark ejecta is composed of fresh mare-like material but may contain minor amounts of highland debris. The bright ejecta is dominated by fresh highland material but minor amounts of mare-like material may be present in some areas.

It is important to determine the source of the mafic material that was excavated and emplaced by the Buch B impact event. Three possibilities seem most likely: 1) a pre-existing mare pond, 2) a cryptomare deposit, and 3) a buried igneous intrusion of basaltic composition.

Although no mare basalt deposits have been identified in the Maurolycus region, it is at least possible that a mare pond existed in the Buch B pre-impact target site. The target site was centered on the rim crest of Buch C crater and the Buch B impact event excavated both wall and elevated rim material. It seems unlikely that any but the smallest ponds could have accumulated in this topographic setting. The volume of the mare pond material would be far too small to account for the large amount mafic material in the Buch B ejecta deposts.

Ancient mare basalt deposits that have been hidden or obscured by superposed higher albedo material are referred to as cryptomaria [*Head and Wilson*, 1992; *Head et al.*, 1993; *Antonenko et al.*, 1995]. Most represent a

record of the earliest (> 3.8 Ga) mare volcanism but some are younger (< 3.8 Ga) mare deposits with surfaces that have been either covered by or contaminated with highland-rich ejecta from near by large impact craters. Studies of the Apollo orbital geochemistry data sets and telescopic near-infrared spectra have shown that mafic geochemical anomalies on the lunar surface are commonly associated with light plains deposits that exhibit dark-haloed impact craters which excavated ancient mare basalts [*e.g.*, *Schultz and Spudis*, 1979, 1983; *Hawke and Spudis*, 1980; *Hawke and Bell*, 1981; *Hawke et al.*, 1985; *Blewett et al.*, 1995; *Antonenko et al.*, 1995]. *Schultz and Spudis* [1979] noted that the excavation of either buried mare basalts or mafic igneous intrusions can produce DHCs and described the difficulties in distinguishing between the two possibilities. Subsequent studies of impact DHCs and cryptomaria have concluded that the vast majority of known DHCs excavated buried mare deposits. Still, some DHCs may have excavated mafic intrusions with basaltic compositions.

Buch B doesn't exhibit the characteristics typical of DHCs that have excavated buried mare basalts. It is an isolated DHC and is not located on a light plains deposit. The asymmetry of the dark exterior deposits suggests the nonuniform distribution of the buried mafic unit. Perhaps an igneous intrusion was present in a portion of the Buch B pre-impact target site. Although a cryptomare origin cannot be ruled out, the bulk of the topographic, geologic, and remote sensing evidence supports an intrusive igneous origin for mafic unit excated and emplaced during the Buch B cratering event.

Other albedo anomalies have been identified in the Maurolycus region [*e.g.*, *Scott*, 1972]. *Scott* [1972] noted that dark rays extend locally from Maurolycus A and suggested a volcanic origin for these features. Maurolycus A is an Eratosthenian-aged crater (diameter = 15 km) located largely on the south wall of Maurolycus crater. *Giguere et al.* [1998] and *Hawke et al.* [1998] noted that portions of the ejecta deposits of Barocius M and Maurolycus B appear slightly darker than typical highland surfaces. These workers suggested that FeO enhancements were associated with these craters as well as Maurolycus A [*Giguere et al.*, 1998; *Hawke et al.*, 1998]. These early results were based on studies of low-resolution (35 km/pixel) FeO maps [*Lucey et al.*, 1995]. In some regions, these large pixels included shadowed areas on slopes that face away from the sun. The inclusion of a small shadowed area would have resulted in a higher FeO value for the entire pixel.

In order to further investigate the possible FeO enhancements associated with these three craters, we utilized higher resolution (1 km/pixel and 125 m/pixel) FeO images. Small FeO enhancements are seen in portions of the ejecta deposits associated with these craters. Still, these enhancements do not approach the FeO values (12 – 14 wt. %) exhibited by the low-albedo exterior deposits of Buch B and they do fall within the range of FeO abundances (5 – 9 wt. %) determined for typical highland units in the Maurolycus region. Maurolycus A and the other craters may have excavated mafic material from depth and incorporated this debris into portions of their ejecta deposits. However, the presence of a basaltic component is not required and it cannot be

concluded that either cryptomare or mafic intrusions were present in the target sites of these craters.

Conclusions

1. A striking albedo anomaly is associated with Buch B crater which is located in the Maurolycus region. This Copernican-aged crater exhibits a dark halo and dark rays.

2. The results of a morphologic analysis clearly indicated that Buch B is an impact structure. It is not a volcanic vent and is not the product of relatively recent volcanic activity.

3. The high infrared eclipse temperatures and the enhanced 3.8 cm radar returns associated with Buch B indicate a high abundance of fresh rocks and fragments in the 1-50 cm size range. The optical maturity image shows that ejecta deposits of Buch B are immature. No abnormally mature areas are associated with the ejecta deposits. Hence, glassy impact melt plays no role in producing the dark deposits associated with Buch B.

4. There is a good correlation between Buch B low-albedo exterior deposits and areas with high FeO values (12 - 14 wt. %). These values are only slightly lower than those exhibited by lunar mare basalts (15 - 18 wt. %). Five point spectra extracted for different portions of the dark deposits are very similar to those collected for fresh mare craters. The dark ejecta is composed of immature mare-like material but may contain minor amounts of highland debris.

5. Buch B excavated either an isolated cryptomare or much more likely, a mafic intrusion. A dike of basaltic composition is the most likely candidate.
6. Maurolycus A, Maurolycus B, and Barocius M may have excavated mafic material from depth and incorporated this material into their ejecta deposits. However, the range of FeO abundances exhibited by these deposits can be explained by known highland rock types in the Maurolycus region.

Chapter 3: Remote sensing studies of the Lomonosov-Fleming basin region of the Moon

Introduction

The Lomonosov-Fleming region is an ancient impact basin on the east side of the Moon. The basin, which is one of the oldest on the Moon, is just out of view from Earth at 19º north, 105º east and is positioned east and northeast of Mare Marginis (Figure 11 and 12). A number of unusual features exist in the Lomonosov-Fleming region, including: bright swirls, groove-like crater chains, dark halo craters, and a concentration of light plains deposits. This 620 km, pre-Nectarian basin is named for the Nectarian-aged crater Fleming (130 km, 15º N., 109.5º E.) and the lower Imbrian-aged crater Lomonosov (93 km, 27.5º N., 98º E.) which is mare filled. Possible overlying basin deposits include those of Imbrium, Crisium, Orientale and Humboldtianum. There are no underlying basins detected. The basin was originally detected by mapping mounds, ridges, and scarpes in the area. No interior ring is observed but the basin does contain Nectarian and Imbrian age light plains (Head and Wilson, 1992; Wilhelms, 1987; Wilhelms and El Baz, 1977). The degraded Lomonosov-Fleming basin has unusual topography (Nozette *et al.*, 1994; Wilhelms and El Baz, 1977). This feature appears as a quasi-circular, smooth plateau of nearly constant elevation about 500 km across (Spudis, 1995). Such an expression of topography is likely caused by infilling of the basin with ancient mare basalts, covered by highland plains and reexposed as the ejecta of dark halo impact craters (Schultz and Spudis, 1979; Schultz and Spudis, 1983). This

interpretation is supported by the mafic signature of the plains in this region in the Clementine global color image (Lucey *et al.*, 1994) and the presence of elevated amounts of Fe in the highland crust here (Lucey *et al.*, 1995). A cluster of dark halo craters occurs in a smooth plains region centered within the basin and were first identified by Wilhelms and El Baz (1977) as older mare material (Im_1) and later revised to be dark halo craters by Wilhelms (1987) based on work by Schultz and Spudis (1979).

Studies of the Apollo orbital geochemical data sets (Hawke and Spudis, 1980; Hawke *et al.,* 1985, Clark and Hawke, 1987; Clark and Hawke, 1991) and Mariner 10 data sets (Robinson *et al.*, 1992) have shown that mafic geochemical anomalies on the east limb and farside of the Moon are commonly associated with light plains deposits that exhibit dark-haloed craters. Geochemical anomalies and other variations in the lunar surface chemistry have been attributed to lateral heterogeneities produced by the chemical differentiation of the global magma ocean, however, other processes are capable of producing geochemical anomalies in the lunar highlands (Hawke and Spudis, 1980):

- Basin-forming impact – large objects that impacted near the end of crustal formation may have produced localized melting and lateral chemical heterogeneities.

- Highland volcanism – Early pre-mare or highland volcanism (>4.0 – 4.1 by) were probably disrupted and largely destroyed during the terminal bombardment of the lunar surface.

- Mare volcanism – Early mare volcanic deposits emplaced before the end of the terminal bombardment would have been thoroughly reworked and mixed with highland material (Ryder and Taylor, 1976). Morphologic evidence of the basalts would be erased and only the geochemical signature would remain to influence the remotely sensed surface composition. Later mare basalts may have been buried by layers of highland debris and described as light plains. Dark halo craters expose the underlying ancient mare deposit (Schultz and Spudis, 1979; Hawke and Spudis, 1980).

- Pyroclastic deposits – These endogenic deposits in regions of explosive volcanic activity are capable of producing areas of mare-like chemistry.

The Lomonosov-Fleming basin is a complicated area and may incorporate several of these processes.

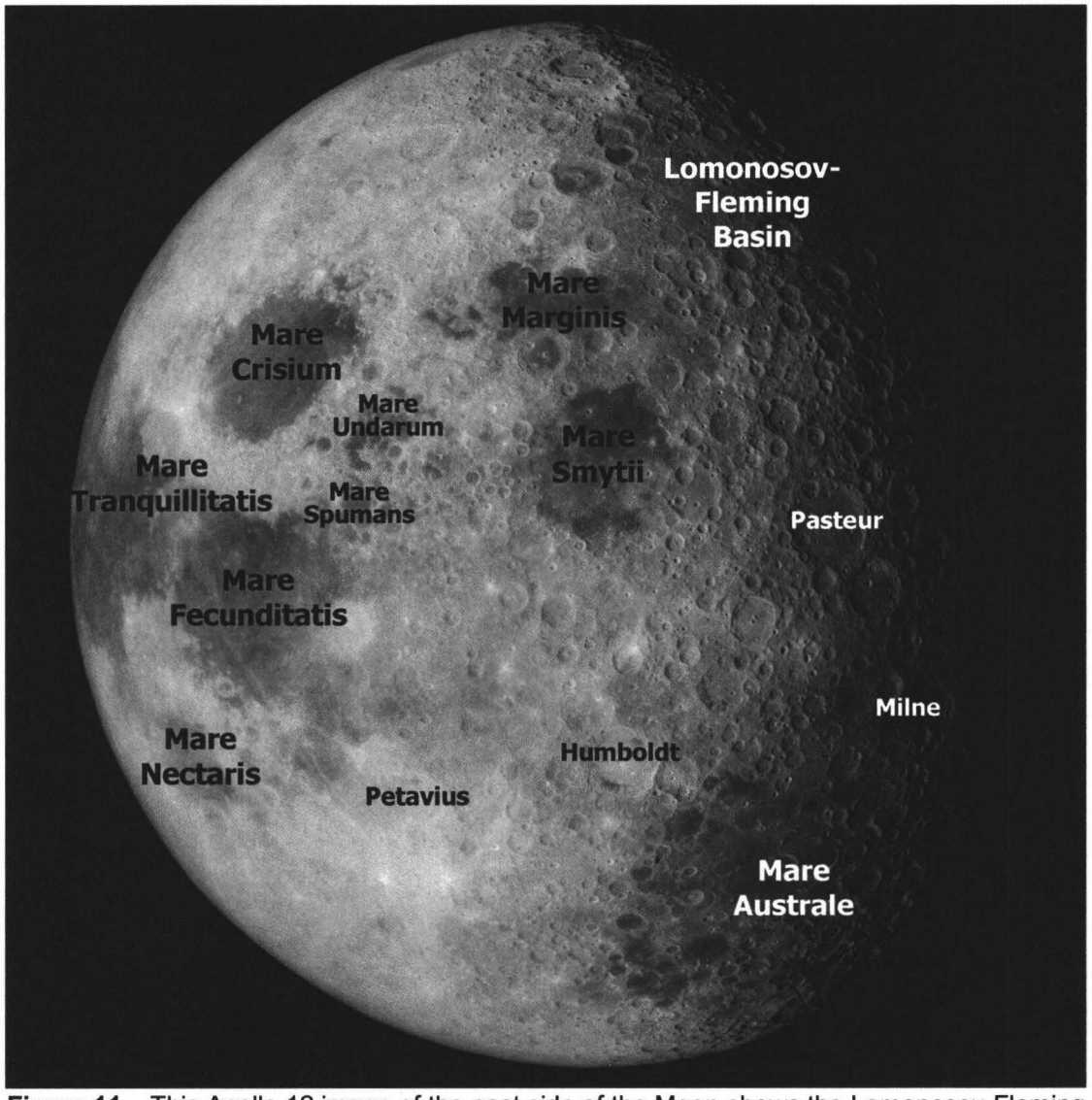

Figure 11 – This Apollo 12 image of the east side of the Moon shows the Lomonosov-Fleming basin on the terminator. Major features are marked for orientation. NASA photograph: AP12-55-8226.

Cryptomaria are ancient mare basalts deposits that are hidden or obscured by superposed higher albedo material (Head and Wilson, 1992; Antonenko *et al.,* 1995; Head *et al.,* 1993). As such, they represent a record of the earliest mare volcanism, and may make a significant volumetric contribution to the lunar crust. Dark halo deposits surrounding craters, commonly referred to as Dark halo craters (DHC's), are one of the primary indicators of the presence of a

cryptomaria. All dark halo deposits were once thought to be volcanic in origin prior to the availability of spacecraft based imagery (Shoemaker, 1962; Schmitt *et al.*, 1967; Salisbury *et al.*, 1968). Some of the dark halo craters were confirmed to have volcanic origins, for example, the dark halo craters on the floor of Alphonsus (Heacock *et al.*, 1966; Carr, 1966, 1969; Hartmann, 1967; Howard and Masursky, 1968; McCauley, 1969; Head, 1976; Peterfreund, 1976; Head and Wilson, 1979). Other dark halo craters are exogenic or impact created craters. The dark halo may have several origins. Some dark halo deposits are composed of impact melts (Howard and Wilshire, 1975; Hawke and Head, 1977, 1979; Hawke *et al.*, 1979a, 1980; Smrekar and Pieters, 1985), whereas other dark halo are derived from the excavation of dark mare basalt material from beneath lighter highlands material (Schultz and Spudis, 1979, 1983; Hawke and Bell, 1981; Bell and Hawke, 1984).

Previous remote sensing and geologic studies have provided evidence for the distribution of ancient mare deposits. Schultz and Spudis (1979) studied the distribution of dark-haloed impact craters in the lunar highlands, most of which appear to have excavated dark mare basalt from beneath a higher albedo surface layer. They suggested that basaltic volcanism predated the last major basin-forming impacts and that early mare volcanism may have been widespread. Hawke and Bell (1981, 1984) used near-IR spectra to demonstrate that many dark-haloed impact craters excavated ancient mare units buried by basin and crater ejecta. In recent years, both Earth-based and spacecraft remote sensing data have been used to characterize selected lunar cryptomaria

(Antonenko *et al.* 1995; Head *et al.* 1993; Blewett *et al.* 1995a; Blewett *et al.* 1995b, Hawke, *et al.,* 1993). Giguere *et al.* (1998; 2000) used maps of FeO and TiO_2 abundances produced from Galileo and Clementine multispectral images coupled with the nearside geologic map in a GIS dataset to investigate the nature and origin of ancient buried mare basalts on the lunar nearside.

The Lomonosov-Fleming basin has been suspected of being the site of a cryptomare for over twenty years (Schultz and Spudis, 1979; Robinson *et al.*, 1992). Th deconvolution modeling studies by Haines *et al.* (1978) allowed the identification of a region north (east) of Mare Smythii with Th concentrations well above average highland levels (Hawke and Spudis, 1980). Still, many issues remain unresolved.

The Clementine multispectral images provide global coverage for the Moon. This dataset permits the reexamination of suspected cryptomare sites on the lunar farside. The focus of this study is the Lomonosov-Fleming basin. The goals of this study include the following: 1) to determine the origin and distribution of dark halo craters in the region, 2) to study the composition of surface units in and around the LF basin region, 3) to search for possible cryptomare and investigate the processes responsible for their formation, 4) to determine the composition of the buried mare unit and investigate whether or not these compositions vary from place to place within the basin, and 5) to investigate the processes responsible for the formation of the Lomonosov-Fleming light plains deposits.

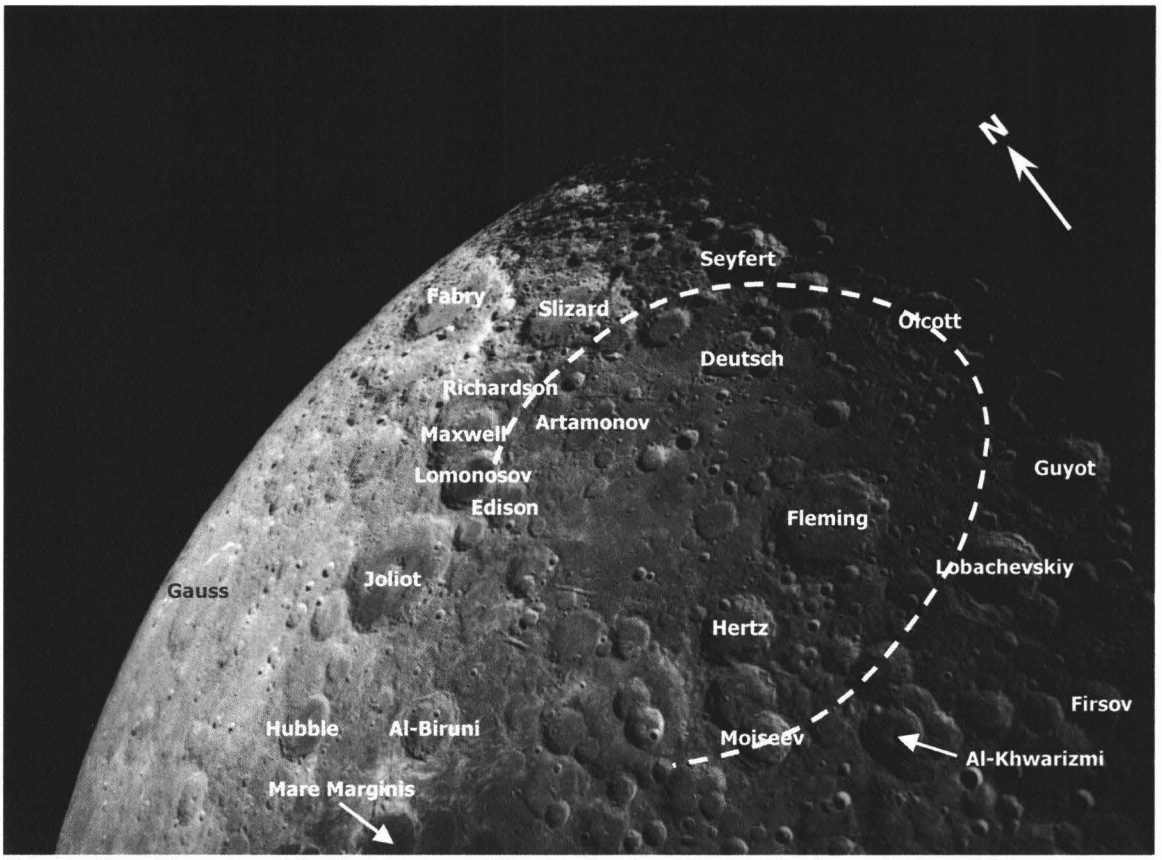

Figure 12 – Close-up of the Lomonosov-Fleming basin. The highly degraded partial basin ring is marked as a white-dotted line (Wilhelms and El-Baz, 1977). Light plains and major dark halo craters are visible in the interior of the basin. NASA photograph: AP12-55-8202.

Methods

The primary data product used for this research were the CD-ROM based Clementine five-color UV-VIS digital image model (DIM) for the Moon published by the U.S. Geological Survey's Astrogeology Program in Flagstaff, Arizona, USA (Eliason *et al.*, 1999; Isbell *et al.*, 1999; Robinson *et al.*, 1999). This calibrated data served as the basis for the production of a number of other data products used in this paper for the Lomonosov-Fleming region.

The visible light (750 nm) images are extracted directly from the digital image model and required only minimal histogram stretching for presentation. The FeO maps were prepared using the algorithms of Lucey *et al.* (2000a). The

Lucey method for mapping FeO content relies on 750 nm reflectance and 950/750 nm ratio images to measure the spectral effects of ferrous iron in major lunar minerals such as pyroxene and olivine. The technique controls for the competing effect of the submicroscopic metallic iron that is produced as rocks are exposed to micrometeorite bombardment and solar wind implantation at the lunar surface (Blewett and Hawke, 2001). The TiO_2 maps were prepared using the algorithms of Lucey *et al.* (2000a) and utilize a parameter derived from 750 nm reflectance and 415/750 nm ratio images. The mapping from the color-albedo parameter to wt. % TiO_2 is based on an understanding of the spectral effects of the Ti-rich opaque mineral ilmenite ($FeTiO_3$) as a component of a mineral mixture comprising the lunar regolith at the locations sampled by Apollo and Luna (Blewett *et al.*, 1997; Lucey *et al.*, 1998, 2000a; Blewett and Hawke, 2001). Optical maturity images were produced using the algorithms of Lucey *et al.* (2000b) to provide information on relative maturity for the study areas. Both 1 km and 100 m resolution images were generated for the region.

Past nearside studies have had the advantage of using detailed ground-based spectra for the analysis of dark halo craters (e.g., Hawke and Bell, 1981; Hawke *et al.*, 1989; Blewett *et al.*, 1995a). Near-infrared spectra as described by McCord (1981) and Bell and Hawke (1984) provide detailed mineralogical information on dark halo deposits. Farside studies such as this one must rely on spacecraft gathered data. High-resolution spectral data is not available, however recent efforts have been documented which allow reliable comparisons to be made between Clementine five-point spectra of different regions (e.g., Tompkins

and Pieters, 1999). These simplified spectra may be used to derive several diagnostic parameters such as: reflectivity, continuum slope, shape and strength of the mafic "1 μm" absorption feature (e.g., Gillis and Spudis, 2000; Hawke *et al.*, Submitted).

Results

Dark halo craters have been identified and mapped in the Lomonosov-Fleming region (Figure 13). The dark halo craters identified are listed in Table 4. Schultz and Spudis (1979) surveyed the global occurrence of dark-halo craters in non-mare terrain with the hope of revealing significant new information on previously unrecognized basaltic units. They used several criteria to standardize the DHC's that were used for the map (e.g., larger that 1 km, must be visible in wide-coverage views to minimize photometric anomalies, bright ray craters are avoided). The survey revealed the widespread occurrence of DHC's on non-mare units. Several prominent DHC's within the Lomonosov-Fleming basin appear on the Schultz and Spudis (1979, Figure 16) dark halo crater map. In this study we positively identified seventeen dark halo craters in the area (Figure 13a).

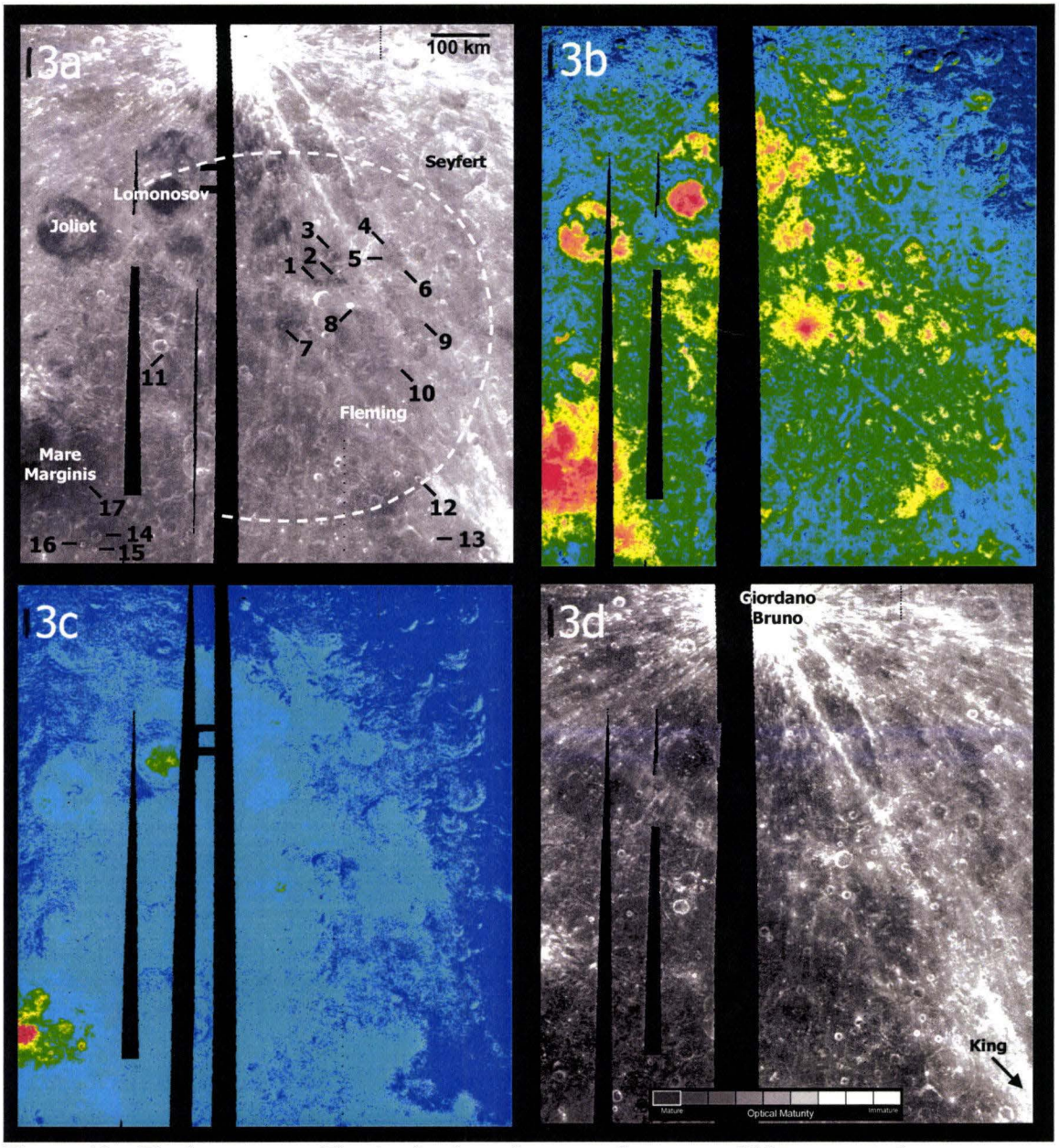

Figure 13 – The Lomonosov-Fleming basin and surrounding area. All images are the same scale and are derived from Clementine 1 km resolution data. 13a – 750 nm visible light image, The Dark Halo Craters listed in Table 4 are identified. The Lomonosov-Fleming basin ring is shown as a white-dotted partial ring (Wilhelms and El-Baz, 1977). 13b – FeO image. 13c – TiO_2 image. 13d – Optical Maturity image.

Legends:

13b - FeO Scale: 0-2: black, 2-4: dk blue, 4-6: cyan, 6-8: green, 8-10: yellow, 10-12: lt orange, 12-14: dk orange, 14-18: red, 18+: white.

13c - TiO_2 Scale: 0-1: blue, 1-2: gray-blue, 2-3: cyan, 3-4: green, 4-5: yellow, 6-7: orange, 7-8: red.

Origin and Distribution of dark halo craters

The criteria used to positively identify dark halo impact craters is derived from Schultz and Spudis (1979) and Head and Wilson (1979). It is important to distinguish endogenic craters which may have dark halos from exogenic impact craters. Head and Wilson (1979) described exogenic craters as generally circular, have a depth/diameter ratio of about 1:5 for fresh craters smaller than 10 km, the presence of braided ejecta facies and secondary craters, and an uplifted rim. Endogenic craters have a noncircular shape, alignment with rilles, fractures or other lineaments absence of a raised rim and crater rays, untextured ejecta deposits, no secondary craters, and a depth/diameter ratio that is generally less than that of impact structures. Extensive efforts have been made to describe the characteristics of endogenically produced pyroclastic deposits (Gaddis *et al.*, 1985; Hawke *et al.*, 1989) and differentiate them from exogenically produced dark halo craters. Hawke *et al.* (1985) described additional criteria for identifying endogenic versus exogenic by using remote sensing data to determine if impact glass or volcanic glass is present.

These criteria were applied to the craters in the Clementine high-resolution (100 m) images and confirm the impact origin of the identified dark halo craters. These craters were further examined, as some dark halos surrounding impact craters are potentially deposits of impact melts (Howard and Wilshire, 1975; Hawke and Head, 1977, 1979; Hawke *et al.*, 1979, 1980; Smrekar and Pieters, 1985). These impact deposits may be recognized by their preferential concentration in topographic lows (Schultz and Spudis, 1979), the presence of cracks and fluid flow features (Hawke and Head, 1977), and a spectral signature

indicative of highland compositions (Bell and Hawke, 1984). Impact melt deposits are generally confined to narrow zones near the rim crest and are surrounded by normal albedo ejecta deposits (Bell and Hawke, 1984). Schultz and Spudis (1979) note that albedo contrasts between impact melts and ejecta deposits decrease rapidly with time, thus misidentification of impact melts as basaltic dark halos should only be of concern for very young craters (Antonenko *et al.*, 1995). The craters identified in Figure 13a do not exhibit impact melt deposits in their dark halos.

Dark, mafic material was excavated from beneath a higher-albedo surface layer by the crater impacts both within and outside the Lomonosov-Fleming basin. The geochemical properties of the dark halos are distinct from the surrounding areas.

The majority of dark halo craters are located within the Lomonosov-Fleming basin (Figure 13a). The largest concentration is found in the northeast quadrant of the basin, primarily within crater Deutsch and in the pre-nectarian/nectarian aged partly mantled terra material immediately to the west. The most prominent dark halo crater (Table 4 – crater 7), also mapped by Schultz and Spudis (1979) lies just north of the center of the basin. Of the dark halo craters that lie outside of the basin, one is located on the southern rim of crater Lobachevskiy and the remaining four lie just to the east of Mare Marginis.

Composition of dark halo craters

The dark halo craters in the Lomonosov-Fleming region have excavated mafic material with FeO values of between 10 and 16 wt. % (see Table 4). These values approach those of typical nearside mare basalts (16 – 21 FeO wt. %). The dark halo crater deposits within the basin range from low to high FeO values. The prominent dark halo crater (Table 4 – crater 7) in the center of the basin approaches a value of FeO 16 wt. %. With the exception of the dark halo crater on the south rim of Lobachevskiy (Table 4 – crater 13), all of the dark halo craters outside of the basin have relatively high FeO values. There appears to be no correlation between the size of the dark halo crater and the FeO value of the material excavated.

Table 4: Dark Halo Geochemical values for craters shown in Figure 13a. These values are peak values for the dark halo. They are derived by averaging a 2x2 pixel matrix around the area of highest geochemical concentration.

Crater Number	FeO	TiO_2
1	13.7	1.7
2	13.9	1.4
3	11.8	0.4
4	13.3	1.6
5	12.6	1.3
6	10.8	1.0
7	15.8	3.6
8	12.3	0.9
9	13.4	1.7
10	12.7	1.5
11	11.3	0.7
12	12.0	0.8
13	10.1	0.6
14	13.5	1.3
15	13.2	0.7
16	14.6	1.5
17	16.3	4.0

These same dark halo craters have excavated material with TiO_2 values of between 0.4 and 4 wt. % (see Table 4). The low end of this range is close to the highlands background value. The high end of the TiO_2 range (4 wt. %) is higher than that of any other known dark halo crater ejecta. The dark halo craters within the basin range from low to high TiO_2 values, similar to the FeO values. The crater marked 17 in Figure 13a has the highest FeO and TiO_2 values in the region.

Figure 13d shows the relative maturity for the Lomonosov-Fleming basin. Bright features are less mature than dark features. The two most prominent impact events visible in this figure occurred to the northwest and southeast of the basin. Impact crater Giordano Bruno has a strong set of immature ejecta rays that reach to the basin to the south and beyond. Impact crater King also has immature rays extending north well into the confines of the basin. The majority of dark halos associated with the dark halo craters are not bright in this image indicating that the halos are fully mature. Thus, the dark color is due to the composition of the darker mare material being excavated and not due to any maturity effects. The most prominent dark halo crater (Table 4 – crater 7) has an ejecta blanket that is brighter than the background (Figure 13d and Figure 18d). The halo on this crater has not completely matured out and will grow even darker in time. Craters must be sufficiently old to permit the soil making up the upper part of the ejecta deposit to mature (Schultz and Spudis, 1979; Hawke and Bell, 1981). An immature dark halo crater may appear bright until the combined

effects of space weathering cause the soil of the halo to darken (Pieters *et al.*, 1993).

Dark halo crater spectra

In order to further investigate the composition of dark halo craters in the Lomonosov-Fleming region, five point spectra were extracted from calibrated and registered Clementine UV-VIS images (*Robinson et al.*, 1999; *Isbell et al.*, 1999; *Eliason et al.*, 1999) using the techniques described by *Tompkins and Pieters* (1999). Spectral reflectance data may be used to derive geochemical and mineralogical information from the lunar soils (Hawke *et al.*, 1989). Lunar spectra are characterized by a positive continuum slope, or overall increase in reflectivity toward the longer wavelengths. A mineral's "signature" is displayed as a residual absorption feature that is superposed on the positive continuum (McCord *et al.*, 1972). The energy of these absorption bands (measured in wavelengths) is determined by the electronic configuration of transitional element ions (e.g. Fe^{2+}, Fe^{3+}, Ti^{3+}, Ti^{4+}) and by the geometry of the coordination sites of their host minerals (Burns, 1970a). The dominant absorption feature for lunar materials has a wavelength centered near 1.0 um and is primarily due to Fe^{2+} crystal field transitions in distorted octahedral coordination sites (Adams, 1974; Gaddis *et al.*, 1985). Four materials commonly found in the lunar soils may contribute to the 1.0 um band: olivine, Fe^{2+} bearing volcanic glasses, orthopyroxene, and clinopyroxene (Hawke *et al.*, 1989).

Orthopyroxene absorption bands are centered between 0.90 to 0.94 um and 1.8 to 2.1 um (Adams, 1974; Hazen *et al.*, 1978). Orthopyroxene is one of the

major mafic minerals associated with lunar highland materials. Spectra characteristic of clinopyroxene have absorption bands centered longward of 0.95 to 1.05 um and 1.8 to 2.2 um. These features are characteristic of spectra obtained for the lunar maria and are caused by the presence of abundant calcium-rich clinopyroxene in the soils (Hawke *et al.*, 1989).

The major absorption feature for olivine is in some ways similar to a homogeneous Fe^{2+} bearing glass band. Both are broad, relatively weak, and centered slightly beyond 1.0 um (Gaddis *et al.*, 1985). Olivine, has a 1.0 um Fe^{2+} feature that is a composite of three distinct, superimposed absorption bands (Burns, 1970b, 1974). Laboratory studies by Singer (1981) showed that the characteristic olivine 1.04 um absorption band is obscured by pyroxene absorption bands unless the sample contains more than 70% olivine. The presence of olivine can be detected at lower levels of concentration by distortions to the long-wavelength edge of the pyroxene band (Singer, 1981; Gaddis *et al.*, 1985).

Spectra were obtained for the ejecta deposits associated with fresh impact craters in the highlands to the north and northeast of the Lomonosov-Fleming basin. The sites where the spectra were obtained were selected as close to the basin as possible to minimize the effects that different lighting conditions could have on absolute reflectance. The craters may expose material dominated by noritic anorthosite or anorthositic norite. The fresh highland spectra shown in Figure 14 were obtained for immature noritic anorthosite lithologies. A spectrum for the exterior deposits of a relatively young impact crater in a mare region is

shown in Figure 14. It exhibits a "1 μm" absorption features and the band shape indicates a mafic assemblage dominated by high-Ca clinopyroxene.

Spectra were extracted for two dark halo craters in the Lomonosov-Fleming basin. They were extracted from the dark exterior deposits surrounding the craters. These spectra are shown in Figure 14. The small dark halo crater on the floor of crater Deutsch (Table 4 – crater 4, Figure 14 - ◆) has a higher reflectance value than the prominent dark halo crater in the center of L-F basin (Table 4 – crater 7, Figure 14 - ▲). This indicates greater contamination of the dark halo with higher albedo highland material. These spectra have relatively strong "1 μm" absorption bands and have band parameters that suggest the dominance of high-Ca pyroxene. The spectra are very similar to that collected for the fresh mare crater and the dark material for which the spectra were obtained are composed of immature mare basalt or immature mare basalt contaminated with varying amounts of highland debris.

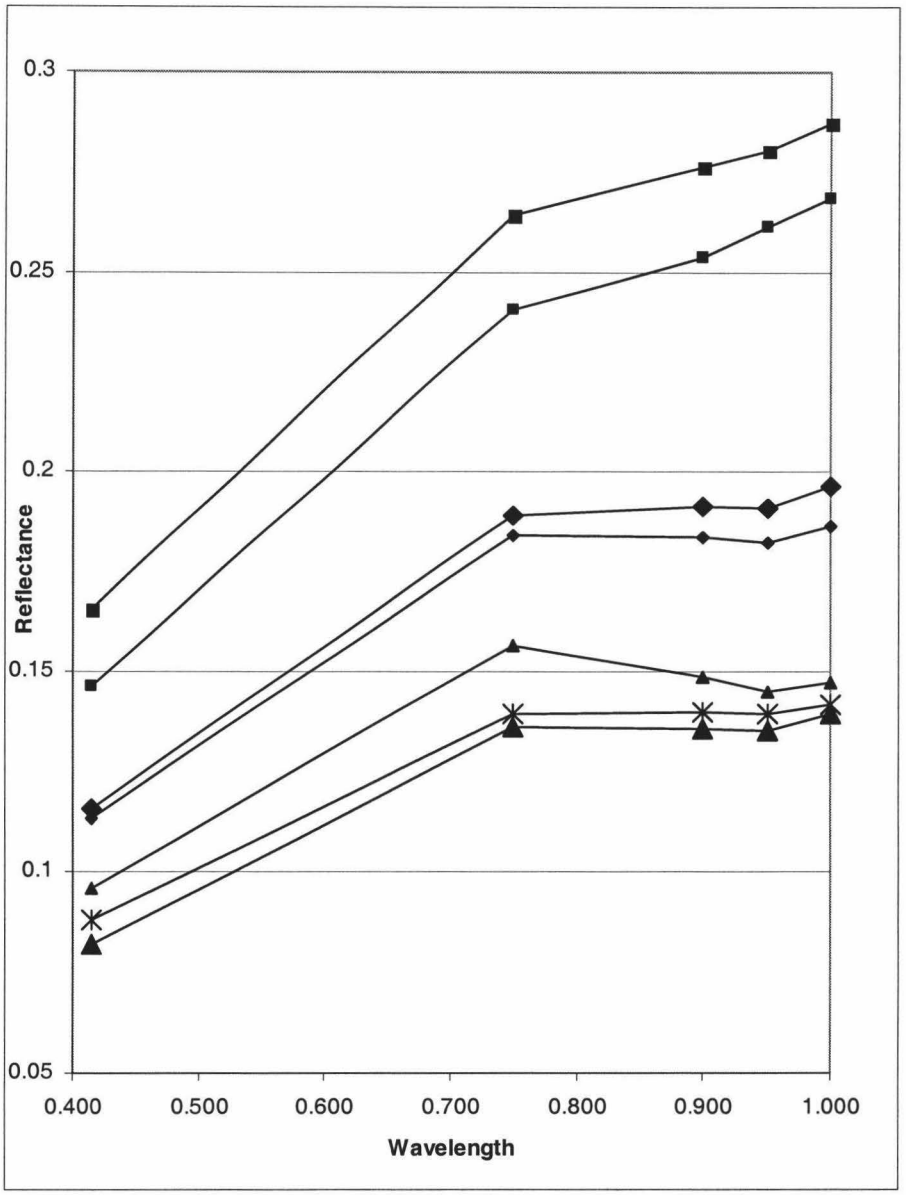

Figure 14 – Five point spectra taken from the Clementine 1 km dataset. The spectra are gathered in pairs with according to the following legend:

▲ – Prominent dark halo crater in the center of L-F basin (Table 4 – crater 7)

◆ – Small dark halo crater on the floor of crater Deutsch in the northwest corner (Table 4 – crater 4)

* – Fresh mare material

■ – Fresh highland material

The dark halo craters in the Lomonosov-Fleming region have excavated mare-like material from beneath a higher albedo, overlying surface. These dark halo craters are a key indicator of the existence of an underlying cryptomare. There are mare ponds in the region, however, the widespread distribution of the

dark halo craters indicate that the mare material is not confined to small areas and indeed represents a cryptomare.

Characteristics of mare deposits in the Lomonosov-Fleming region

In this study, we used relative albedo values and geochemical data to characterize the mare deposits in or near the Lomonosov-Fleming basin. Mare ponds in the Lomonosov-Fleming region generally have lower FeO values than typical nearside mare basalts in the major basins. One explanation is the small size of the mare deposits as compared to nearside deposits. The lateral transport of material easily contaminates a mare deposit with small spatial extent. Also of note is that these deposits are thin, which promotes contamination by vertical mixing processes. A third reason for the lower relative values may be attributed to the fact that nearly all of the mare ponds in the region are older (Im_1) than the their nearside counterparts. The exception is crater Lomonosov which has an age of Im_2. The two major maria southwest of Lomonosov-Fleming (Marginis and Smythii) are also composed of Im_2 basalts. The mare and mare ponds are listed in Table 5 along with the peak FeO and TiO_2 values. The older mare deposits tend to have lower FeO and TiO_2 values. These basalts have had more time to be contaminated with low iron highland material.

Table 5: Geochemical values and ages of mare and mare ponds in the Lomonosov-Fleming region as shown in Figure 11 and Figure 12. The geochemical values are peak values for each area and are derived by averaging a 2x2 pixel matrix around the area of highest geochemical concentration.

Name	Longitude[1]	Latitude[1]	Diameter[1]	Age[2]	FeO	TiO_2
Artamonov	103.5E	25.5N	60.0	Im_1	12.6	2.5
Edison	99.1E	25.0N	62.0	Im_1	11.9	1.5
Joliot	93.1E	5.8N	164.0	Im_1	14.2	2.0
Lomonosov	98.0E	27.3N	84.0	Im_2	15.4	3.6
Mare Marginis	86.1E	13.3N	420.0	Im_2	17.2	5.9
Mare Smythii	87.5E	1.3N	373.0	Im_2	17.4	6.0
Maxwell	98.9E	30.2N	107.0	Im_1	12.9	1.9

[1]Adapted from the Lunar Nomenclature Database published by the U.S. Geological Survey Flagstaff Field Center.
[2]Wilhelms and El Baz, 1977

Age, composition, and distribution of cryptomare

The terrain northeast of Mare Smythii is relatively close to the Lomonosov-Fleming basin (< 400 km) and has been identified in the past as having geochemical anomalies and possible cryptomare (Haines *et al.*, 1978; Hawke *et al.*, 1985). The anomalous region has enhanced iron and titanium values in both the Davis and the Metzger versions of the orbital gamma-ray data sets (Metzger and Parker, 1979; Davis, 1980). Anomalies can also be identified in the orbital X-ray data for this region (Schultz and Spudis, 1979; Andre *et al.*, 1979; Clark and Hawke, 1991). The province is dominated by light plains and terra mantling material as described by Wilhelms and El-Baz (1977) these include Imbrian plains (Ip), middle Imbrian to late Nectarian plains (INp), and Imbrian age terra mantling material (It). Schultz and Spudis (1979) and Young *et al.* (1972) identified numerous dark halo craters in the area. The surface composition is intermediate between that of mare basalts and typical lunar highland material.

The region probably experienced an episode of volcanism early (> 3.8 Ga) in lunar history that produced deposits with both mare and KREEP affinities. The surfaces of these basaltic deposits were subsequently contaminated by highland material contributed by later impact events. The addition of highland material would alter the surface composition and raise the low albedos of the volcanic surfaces Hawke *et al.*, 1985).

Still further north-northeast of the terrain just discussed lays the Lomonosov-Fleming basin. Roughly one-third of the area under the basin may be made up of cryptomare (see Figure 15). The largest cryptomare patch begins just west of the center of the basin, and extends east almost to the edge of the basin. This patch extends to the south almost to crater Lobachevskiy and a section of the cryptomare extends to the northwest towards Artamonov. Many of the craters within the basin have cryptomare mapped within them. Good examples include Deutsch, Fleming and Hertz. These areas most likely represent mare ponds that have been obscured by highland material. The majority of the cryptomare mapped in the Lomonosov-Fleming region underlies the light plains material that occupies much of the basin. A lesser amount of cryptomare underlies materials associated with other highland units, such as material of relatively undegraded circular craters, which is the case at Lobachevskiy (Ic_2), Moiseev (Ec), and Espin (pNc).

Most of the material within the Lomonosov-Fleming basin is Nectarian and Pre-Nectarian aged. This includes the light-colored plains material (Np), material of unmantled terra (pNt), and material of partly mantled terra (NpNt). Some

furrowed and pitted material (INfp) is located in the northwest corner of the basin and is variable in age. It may have both Nectarian and imbrium aged units. Patches of Imbrium-aged light-colored plains (Ip) are scattered around the basin and are often found on the floors of the larger craters. Thus, with the majority of units that cover and obscure the underlying basalts having ages in the Nectarian system and occasionally in the pre-Nectarian system the implication is that the cryptomare is quite ancient. The underlying basalts may be among the oldest on the Moon.

Figure 15 – Cryptomare map of the Lomonosov-Fleming region. Legend - Cryptomare associated with Light Plains: yellow, Cryptomare associated with other highland units: purple, Mare basalt: red, Possible pyroclastic origin: orange. The Lomonosov-Fleming basin ring is shown as a white-dotted partial ring (Wilhelms and El-Baz, 1977).

Volcanism was active from 4.3 ba to at least 3 ba (the youngest basalts in the Apollo collection) and unsampled lavas may be younger than 1 ba (Heiken *et al.*, 1991; Spudis, 2001). Lunar samples provide evidence for ancient mare volcanism. Although most of the mare basalts returned from the moon that have been radiometrically dated are younger than about 3.9 by, other samples provide

evidence of earlier volcanism (Schultz and Spudis, 1979). A small percentage of the lithic clasts in some Apollo 14 Fra Mauro breccias suggest the existence of pre-Imbrium mare basalt flows (Ryder and Taylor, 1976). Fragment 14305 has been conclusively dated at 4.23 ±0.05 Ga (Taylor *et al.*, 1983; Shervais *et al.*, 1983). Taylor *et al.* (1983) suggested that mare-type volcanism commenced at least as early as 4.2 Ga in the Fra Mauro region and probably across much of the lunar surface. Numerous single pyroxene and plagioclase clasts in the Apollo 16 breccias display mare basalt affinities and have $^{40}Ar - ^{39}Ar$ ages of 4.1 – 4.25 by (Schaeffer and Hussain, 1973).

Dark halo craters are useful for locating and identifying the extent of cryptomare, however, the information they provide must be interpreted carefully. Dark halo craters commonly occur in clusters, but not all impact craters in areas of known cryptomare exhibit dark ejecta deposts. This observation may reflect the localized occurrences of the buried unit, it thickness, its depth burial, and the subsequent cratering history. Ancient basalts extruded as thin (<100m) pooled units within old craters (as in Mare Australe) can be easily masked in ejecta deposits of subsequent craters owing to the dilution with highland material. Often these deposits are localized which reduces the target area and the possibility of re-exposure. The characteristics of the buried deposit regulate the type and appearance of the resultant dark halo crater. Deeply buried basaltic deposits may result in only near-rim dark halo deposits which may be narrow or discontinuous. Near surface basaltic deposits may be have more distant and dispersed ejecta deposits. Thus, only relatively small craters can reveal thinly

buried basaltic deposits. The balance between crater diameter and thickness and depth of the deposit governs the production of dark halo craters. Since these factors may not always be optimum and dark halo craters may not always exist over buried deposits, the extent of global buried basaltic deposits may generally be underestimated for most cryptomare sites (Schultz and Spudis, 1979), and is quite possibly underestimated at the Lomonosov-Fleming basin as well.

Our analysis with the Clementine data products confirms the existence of an apparent compositional variation of mare basalts in the cryptomare. The dark halo craters have excavated FeO values that vary from 10.8 - 15.8 wt. % and the TiO_2 values vary from 0.4 - 3.6 wt. A trend is observed if the dark halo crater values from Table 4 are plotted (see Figure 16). As the FeO wt. % increases the TiO_2 wt. % correspondingly increases. To the extent these dark halo craters fall on a straight line indicates that the mare basalt that was excavated by the dark halo crater impacts are from the same geochemically uniform unit. The material in the dark halo is first diluted during the original impact and is further diluted by highland material over time, which results in a spreading out of the points along the trend line. The dark halo craters in the lower left of plot in Figure 16 are the most contaminated. Dark halo craters that fall away from the trend line may indicate geochemical variations in the cryptomare composition.

Most nearside mare basalts have maximum FeO values of around 21 wt. % (Lucey *et al.*, 1998). If the trend line were carried out to an FeO value of 21 wt. %, the projected TiO_2 value would be over 5.0 wt. %, assuming that the trend

remains linear. This projected value ranks as an intermediate or high Ti basalt on most scales (see Table 4 in Giguere *et al.*, 2000). The actual TiO_2 value of 3.6 wt. % for dark halo crater #7 is the highest for any lunar cryptomare.

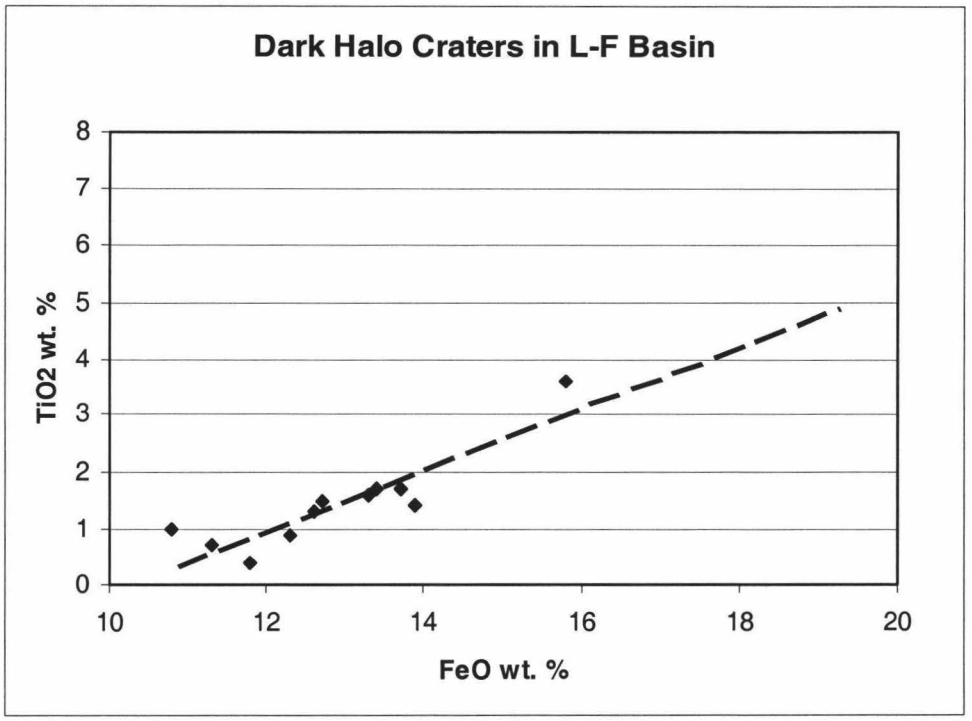

Figure 16 – Geochemical values for the dark halo craters within the Lomonosov-Fleming basin. Generally, the TiO_2 value increases as the FeO increases.

Case studies

The Lomonosov-Fleming basin was examined with high-resolution Clementine (100 m resolution) data. Two areas are presented from this detailed study: the area including crater Deutsch and area to the west (Figure 17), and the prominent dark halo crater in the central Lomonosov-Fleming basin (Figure 18). Crater Deutsch is located in the northeast corner of the basin; this 66 km crater has a smooth light plains interior and contains three dark-haloed craters (Table 4 – craters 4, 5, 6). The FeO values for these three craters range from 10.8 – 13.3 wt. % and the TiO_2 values range from 1.0 – 1.6 wt. %. The area to the west has three dark halo craters (Table 4 – craters 1, 2, 3) which lie in Nectarian and Pre-Nectarian terra material (Wilhelms and El-Baz, 1977). The FeO values are slightly higher than for the dark halo craters within Deutsch and range from 11.8 – 13.9 wt. %. The TiO_2 values range from 0.4 – 1.7 wt. %. The FeO and TiO_2 have elevated values and taken together with the spectra indicate that these impacts have exposed mafic material (Hawke *et al.*, Submitted).

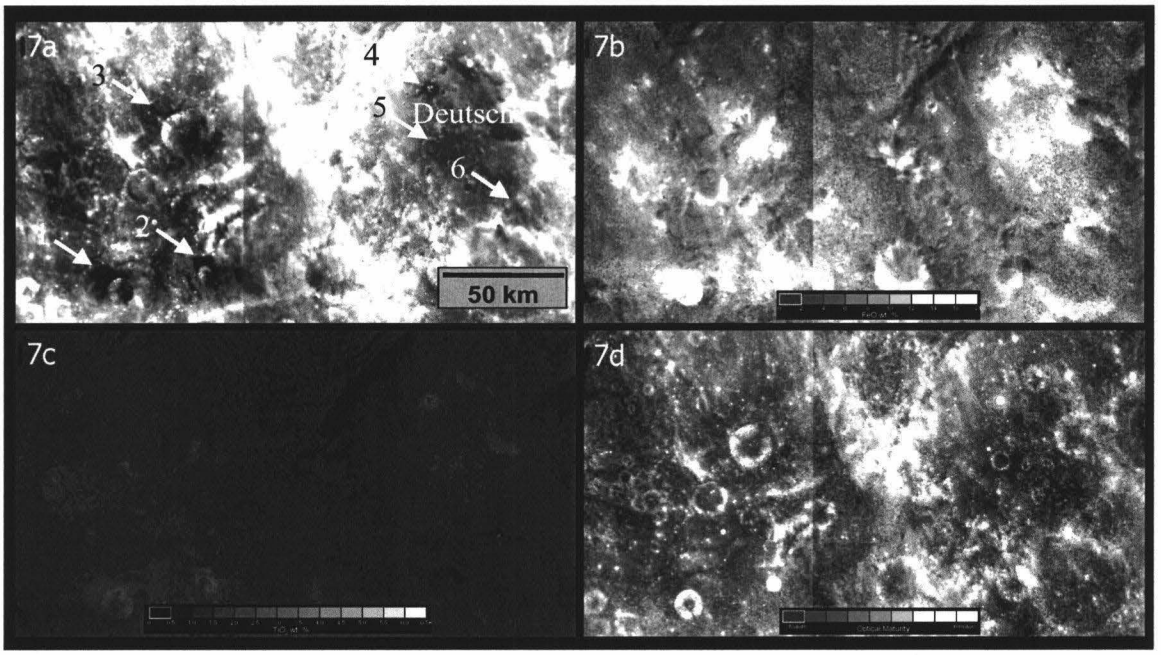

Figure 17 – Dark halo craters in crater Deutsch and the terrain to the west. All images are the same scale and are derived from the Clementine 100 m resolution data. 17a – 750 nm image. 17b – FeO image. 17c – TiO_2. 17d – Optical Maturity image.

The prominent dark halo crater (Table 4 – crater 7) in the central Lomonosov-Fleming basin has the highest FeO and TiO_2 values (FeO 15.8 wt. %, TiO_2 3.6 wt. %) in the basin. Only one crater (Table 4 – crater 17) east of Mare Marginis has higher values. The crater is approximately 7 km in diameter.

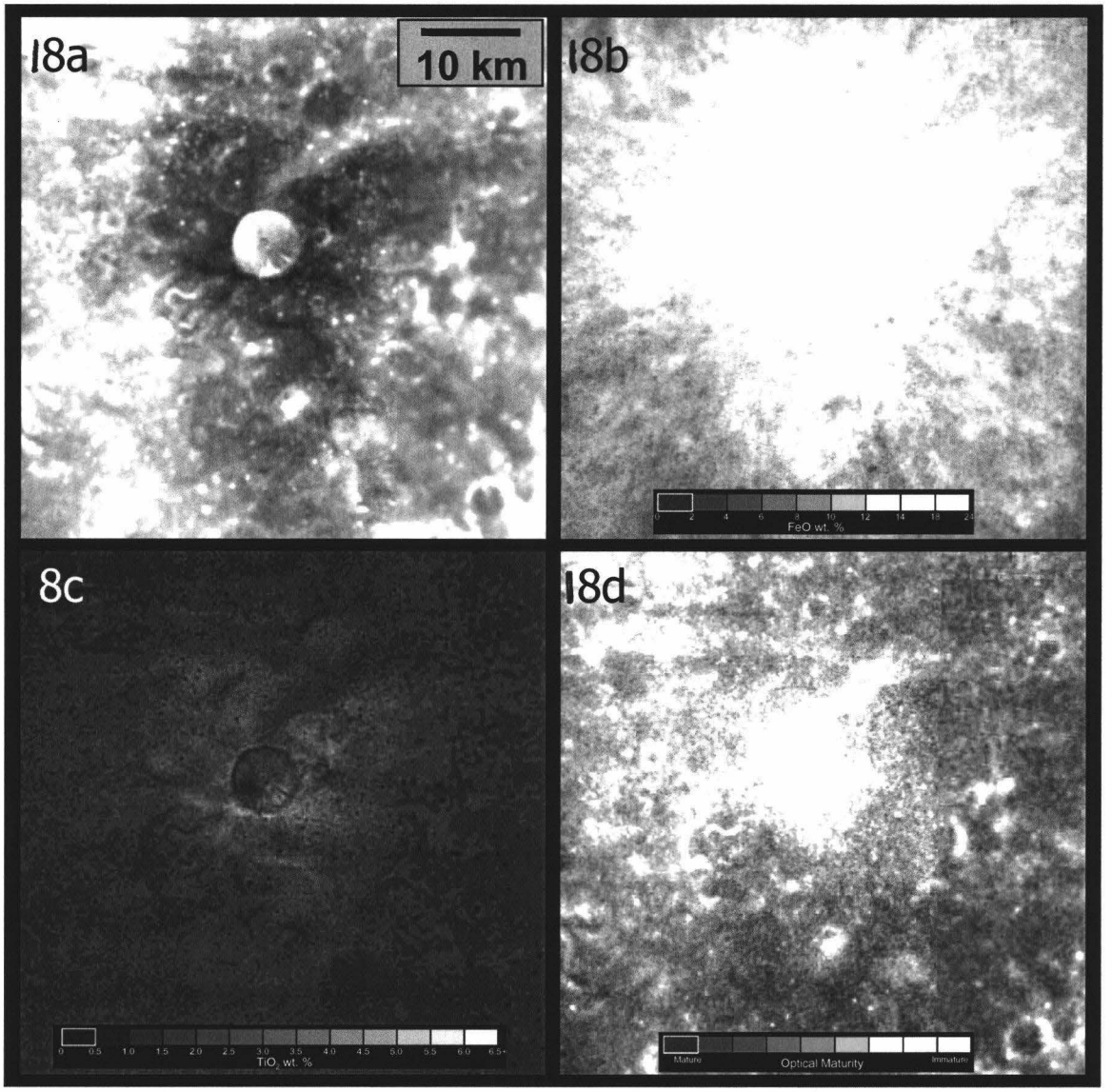

Figure 18 – Prominent dark halo crater in the center of Lomonosov-Fleming basin. All images are the same scale and are derived from the Clementine 100 m resolution data. 18a – 750 nm image. 18b – FeO image. 18c – TiO_2. 18d – Optical Maturity image.

Processes responsible for cryptomare formation

Understanding the processes that are responsible for the formation of cryptomare in the Lomonosov-Fleming basin are challenging due to the ancient age of the mare material in this region. There may have been at least two major processes that contributed to the end result that we observe today: early burial

by a basin-forming impact, and subsequent burial of the mare surfaces by highland-rich ejecta. These proposed processes which may be responsible for the formation of this cryptomare, have been noted in other regions.

In the Schiller-Schickard region remote sensing studies by Hawke and Bell (1981) and Bell and Hawke (1984) have confirmed the hypothesis of Schultz and Spudis (1979) that the dark halo impact craters in the region formed when ancient mare basalts were excavated from beneath a higher albedo plains units emplaced by the Orientale basin-forming impact (Blewett *et al.*, 1995). Wilhelms (1987) lists three overlying basins for Lomonosov-Fleming: Imbrium, Crisium, and Humboldtianum. Imbrium would have deposited only small amounts of material in the basin, due to the great distance of the impact. The groovelike crater chains located on the western side of the basin (Figure 12) may be secondary craters to the Imbrium basin. The Crisium impact (Figure 11) may have deposited a substantial amount of material on the Lomonosov-Fleming region. Humboltianum appears to have most influenced the surrounding region. Wide expanses of Nectarian-aged lineated basin material is mapped around the impact basin and extends to the south toward the Lomonosov-Fleming basin. The Humboltianum impact may have produced an Orientale-like effect on the Lomonosov-Fleming region producing an early burial by a basin-forming impact.

The Balmer basin (68º E, 15º S), exhibits dark-halo craters on a plains unit. The area is surrounded (within 250 km) by five major impact structures of Imbrium or younger age that could have contributed to the thin cover of highland material (Hawke and Spudis, 1980). Rays and secondaries from Langrenus and

other smaller Copernican aged craters have contributed highland material and raised the albedo (Maxwell and Andre, 1981). The subjacent basaltic material would have been mixed with crater material during ejecta emplacement and by subsequent vertical mixing by small impacts that penetrated the thin highland debris surface units (Hawke and Spudis, 1980). Calculations based on ejecta distribution equations presented by McGetchin *et al.* (1973) as well as the presence of secondary crater chains and clusters and rays, indicate that these impacts contributed significant amount of highland material to the Balmer plains units (Hawke *et al.*, 1985). Such a surface would exhibit a higher albedo than an uncontaminated regolith developed on mare basalt (Hartmann and Wood, 1971) and would appear to be a 'light plains' type unit (Hawke *et al.*, 1985). It can be demonstrated that the Balmer basin has been contaminated by highlands ejecta from surrounding craters, it is not clear that this contamination is solely responsible for the high albedo of the Balmer plains units (Hawke *et al.*, 1985). Like the Balmer basin there are many impact candidates that could have contributed highland material to the Lomonosov-Fleming region over the course of its long history. The two most recent examples are clearly visible in the visible light image (Figure 13a) and the optical maturity image (Figure 13d). Giordano Bruno is a Copernican-aged crater that lies north of the basin. The ray system and associated material from this crater extends well into the basin. King crater, also Copernican-aged, is positioned to the southeast of the basin. King's ray structure extends completely across the basin in some places. These two recent

examples and previous impacts around the basin have contributed to the burial of the mare surfaces by highland-rich ejecta.

Light plains can be produced by ballistic erosion and sedimentation processes (Oberbeck *et al.*, 1974; Oberbeck, 1975). Ejecta associated with large cratering events impacts and mixes with the local target material in relatively predictable ways, obscuring pre-impact topography and resulting in the formation of deposits of relatively smooth light plains in low-lying regions. These light plains do not represent an ejecta blanket laid down over the surface, but rather an ejecta deposit which consists of a dynamic mixture of primary ejecta and local material, where the proportion of primary ejecta material to local target material decreases exponentially with radial distance from the primary crater (Oberbeck *et al.*, 1974; Oberbeck, 1975). Multispectral imaging has proved to be useful in identifying cryptomaria since the light plains emplacement process incorporates local material in the eject deposit, which can be recognized by mixing analysis of spectral endmembers (Mustard *et al.*, 1992) or by simply observing elevated geochemical values over typical highland values. The emplacement of highland-rich material on a pre-existing ancient mare surfaces played and important role in the formation of light plains in the Lomonosov-Fleming region and elsewhere on the Moon. The light plains deposits in the basin have elevated FeO values with an average of 7.6 wt. %. For comparison, the surrounding highlands have FeO values around 3.8 wt. %. The light plains in the basin exhibit only slightly elevated TiO_2 values (0.7 wt. %), whereas the surrounding highlands have lower TiO_2 values of 0.4 wt. %.

Conclusions

As described by Hawke and Spudis (1980) thinly buried volcanic deposits are the source of certain geochemical anomalies on the eastern limb and farside and apparently can exert a strong influence on regional surface chemistry. The Lomonosov-Fleming region should be included as a geochemically anomalous area. These geochemical anomalous areas should not be included in attempts to establish average global and regional highland compositions.

Summarizing the major findings of this effort:

1. Dark halo craters in this region are of impact origin. Chemical and spectral data indicate that mare basalts were excavated by these dark halo impact craters. Since mare materials were excavated from beneath a higher albedo, highlands-rich surface units, a major expanse of cryptomare exists in and around the Lomonosov-Fleming basin.
2. Varying amounts of highland debris has contaminated the mare basalts exposed in the dark haloes. The least contaminated mare material exhibits FeO values of 16.3 wt. % and TiO_2 values of 4.0 wt. %.
3. Mare surface units in the Lomonosov-Fleming region are small and appear to be contaminated by highlands material. The maximum FeO values range between 11.9 wt. % and 17.4 wt. %. Maximum

TiO_2 values range between 1.5 wt. % and 6.0 wt. %. Additional contamination of some of these deposits will produce cryptomare!

4. Several deposits of dark mantle material were identified and mapped. This low albedo material mantles and subdues rugged terrain. These dark mantle deposits are most likely to be pyroclastic debris emplaced by explosive volcanic eruptions.
5. Age of ancient mare basalts:
    a. Cryptomare occur beneath surface units of both Imbrian and Nectarian age. However, Nectarian-aged units with subjacent cryptomare are much more extensive than Imbrian-aged deposits with cryptomare.
    b. The bulk of the cryptomare in the Lomonosov-Fleming region was emplaced in pre-Imbrian time.
    c. Volcanism appears to have peaked in pre-Imbrian time in the Lomonosov-Fleming region of the lunar farside. The area covered by mare basalts is far less than the area of the cryptomare.
6. Formation of the cryptomare in the Lomonosov-Fleming region:
    a. Formed by covering ancient mare surfaces with varying thicknesses of highlands debris.
    b. Both impact basins and craters played a role by transporting highlands material to mare surfaces in the Lomonosov-Fleming region.

c. Humboldtianum basin may have played a key role in cryptomare formation in the Lomonosov-Fleming region.

7. Most cryptomare in the Lomonosov-Fleming region are associated with light plains deposits. The existence of flat expanses of ancient mare basalt promoted the development of light plains in the Lomonosov-Fleming region as well as elsewhere on the Moon.

The evidence listed above confirms that the Lomonosov-Fleming region is the site of a major cryptomare. The FeO values in the dark-haloed craters approach the values of surface mare and the TiO_2 values of some of the DHC's are as high as 4.0 wt. %. These values are higher than any other cryptomare on the Moon (Giguere *et al.*, 2001). Although we have taken a comprehensive look at the Lomonosov-Fleming region, future studies with new and existing datasets are worthwhile. A comparison of the geochemical information obtained from the Prospector mission and the Clementine datasets used for this research would extend our knowledge about this area.

References (Chapter 1)

Bell J. and Hawke B. Ray (1995) Compositional variability of the Serenitatis/Tranquillitatis region of the Moon from telescopic multispectral imaging and spectroscopy. *Icarus* **118** 51-68.

Belton M. J. S. and the Galileo SSI team. (1992) Lunar impact basins and crustal heterogeneity: New western limb and farside data from Galileo. *Science* 255, 570-576.

Blewett D. T., Lucey P. G. and Hawke B. Ray (1997) Clementine images of the lunar sample-return stations: Refinement of FeO and TiO_2 mapping techniques. *J. Geophys. Res.* **102** (E7), 16319-16325.

Boyce J. M. (1976) Ages of flow units in the lunar nearside maria based on Lunar Orbiter IV photographs. *Proc. Lunar Planet. Sci. Conf.* ***7th***, 2717-2728.

Boyce J. M. and Johnson D. A. (1977) Ages of flow units in Mare Crisium based on crater density. *Proc. Lunar Planet. Sci. Conf.* ***8th***, 3495-3502.

Basaltic Volcanism Study Project (1981 a) Lunar Mare Basalts. In *Basaltic Volcanism on the Terrestrial Planets*, p 254. Pergamon Press, Inc., New York.

Basaltic Volcanism Study Project (1981 b) Lunar Mare Basalts. In *Basaltic Volcanism on the Terrestrial Planets*, Ch. 2. Pergamon Press, Inc., New York.Campbell B. A., Hawke B. Ray and Thompson T. W. (1997) Regolith composition and structure in the lunar maria: Results of long-wavelength radar studies. *J. Geophys. Res.* **102** (E8), 19307-19320.

Charette M. P., McCord T. B., Pieters C. and Adams J. B. (1974) Application of remote spectral reflectance measurements to lunar geology classification and determination of titanium content of lunar soils. *J. Geophys. Res.* **79**, 1605-1613.

Davis P. A. (1980) Iron and titanium distribution on the Moon from orbital gamma ray spectrometry with implications for crustal evolutionary models. *J. Geophys. Res.* **85**, 3209-3224.

Delano J. W. (1986) Pristine Lunar Glasses: Criteria, Data, and Implications. *Proc. Lunar Planet. Sci. Conf.* ***16th,*** in *J. Geophys. Res.* **91** (B4), D201-D213.

Delano J. W. (1990) Buoyancy-driven melt segregation in the Earth's moon, I. Numerical results, *Proc. Lunar Planet. Sci. Conf.* ***20th***, 3-12.

Dowty E. (1975) Shallow origin of mare basalts. *Conf. on Origins of Mare Basalts*. **234**, 35-39.

Friedman R. C., Blewett D. T., Taylor G. J. and Lucey P. G. (1996) FeO and TiO_2 Variations in Mare Imbrium (abstract). *Lunar Planet. Sci.* **27**, 383-384.

Gillis J. J. and Spudis P. D. (1998) Inventory of FeO and TiO_2 compositions for mare deposits on the far side of the Moon. *Lunar Planet. Sci.* **29**, abstract #1521.

Greeley R., Kadel S. D., Williams D. A., Gaddis L. R., Head J. H., McEwen A. S., Murchie S. L., Nagel E., Heukum G., Pieters C. M., Sunsine J. M., Wagner R. and Belton M. J. S. (1993) Galileo Imaging Observations of Lunar Maria and Related Deposits. *J. Geophys. Res.*. **98** (E9), 17183-17205.

Haskin L. and Warren P. (1991) Lunar Chemistry. In *Lunar Sourcebook* (eds. G. H. Heiken, D. T. Vaniman and B. M. French), pp. 357-474. Cambridge Univ. Press.

Head J. W. (1976) Lunar Volcanism in Space and Time *Rev. Geophys. Space Phys.* **14**, 265-300.

Head J. W., Pieters C. M., McCord T. B., Adams J. and Zisk S. H. (1978) Definition and detailed characterization of lunar surface units using remote observations. *Icarus* **33**, 145-172.

Herbert F. (1980) Time-dependent lunar density models. *Proc. Lunar Planet. Sci. Conf.* ***11th***, 2015-2030.

Hess P. (1991) Diapirism and the Origin of High TiO_2 Mare Glasses. *Geophys. Res. Lett.* **18**, 2069-2072.

Hess P. and Parmentier M. (1995) A model for the thermal and chemical evolution of the Moon's interior: implications for the onset of mare volcanism. *Earth Planet. Sci. Lett.* **134,** 501.

Jaumann R. (1991) Spectral-chemical analysis of lunar surface materials. *J. Geophys. Res.* **96**, 22793-22807.

Johnson T. V., Sanders R. S., Matson D. L. and Mosher J. A. (1977) A TiO_2 abundance map for the northern maria. *Proc. Lunar Planet. Sci. Conf.* **8th**, 1029-1036.

Johnson J. R., Larson S. M. and Singer R. B. (1991) Remote Sensing Of Potential Lunar Resources 1. Near-Side Compositional Properties. *J. Geophys. Res.* **96** (E3), 18861-18882.

Kesson S. E. and Ringwood A. E. (1976) Mare basalt petrogenisis in a dynamic Moon. *Earth Planet. Sci. Lett.* **30**, 155-163.

Longhi J. (1992) Experimental petrology and petrogenesis of mare volcanics. *Geochim. Cosmochim. Acta* **56**, 2235-2251.

Lucey P. G., Taylor G. J. and Malaret E. (1995) Abundance and Distribution of Iron on the Moon. *Science* **268**, 1150-1153.

Lucey P. G., Blewett D. T., Johnson J. L., Taylor G. J. and Hawke B. R. (1996) Lunar Titanium Content from UV-VIS Measurements (abstract). *Lunar Planet. Sci.* **27**, 781-782.

Lucey P. G., Blewett D. T. and Hawke B. R. (1998) Mapping the FeO and TiO2 content of the lunar surface with multispectral imagery. *J. Geophys. Res.* **103** (E2), 3679-3699.

Ma M. S., Schmitt R. A., Nielsen R. L., Taylor G. J., Warner R. D., and Keil K. (1979) Petrogenesis of Luna 16 aluminous mare basalts. *Geophys. Res. Lett.* **6**, 909-912.

McKay D. S., Heikey G., Basu A., Blanford G., Simon S., Reedy R., French B. M. and Papike J. (1991) The Lunar Regolith. In *Lunar Sourcebook* (eds. G. H. Heiken, D. T. Vaniman and B. M. French), pp. 285-356. Cambridge Univ. Press.

Melendrez D. E., Johnson J. R., Larson S. M. and Singer R. B. (1994) Remote Sensing Of Potential Lunar Resources 2. High spatial resolution mapping of spectral reflectance ratios and implications for nearside mare TiO_2 content. *J. Geophys. Res.* **99** (E3), 5601-5619.

Metzger A. E., Johnson T. V. and Matson D. L. (1979) A comparison of mare surface titanium concentrations obtained by spectral reflectance and gamma-ray spectroscopy: An early assessment. *Proc. Lunar Planet. Sci Conf.* **10th**, 1719-1726.

Metzger A. E. and Parker R. E. (1979) The distribution of titanium on the lunar surface. *Earth Planet. Sci. Lett.* **45**, 155-171.

Mustard J. F., Li L. and He G. (1998) Nonlinear spectral mixture modeling of lunar multispectral data: Implications for lateral transport. *J. Geophys. Res.* **103** (E8), 19419-19425.

Neal C. R., Taylor L. A., Hughes S. S. and Schmitt R. A. (1990) The significance of fractional crystallization in the petrogenesis of Apollo 17 Type A and B high-Ti basalts. *Geochim. Cosmochim. Acta* **54**, 1817-1833.

Neal C. R. and Taylor L. A. (1992) Petrogenesis of mare basalts: A record of lunar volcanism. *Geochim. Cosmochim. Acta* **56**, 2177-2211.

Neal C. R. (1999) Mare Sample Data Base, personal communication.

Nozette S. and the Clementine team. (1994) The Clementine Mission to the Moon: Scientific Overview. *Science* **266**, 1835-1839.

Papike J. J., Hodges F. N., Bence A. E., Cameron M., and Rhodes J. M. (1976) Mare Basalts: Crystal Chemistry, Mineralogy, and Petrology. *Rev. Geophys. Space Phys.* **14**, 475-540.

Papike J. J., Graham R. and Shearer C. K. (1998) Lunar Samples. In *Planetary Materials* (eds. J. J. Papike and P. H. Ribbe), p. 5-48. The Mineralogical Society of America.

Pieters C. M. (1978) Mare basalt types on the front side of the Moon: A summary of spectral reflectance data (abstract). *Proc. Lunar Planet. Sci Conf.* **9th**, 2825-2849.

Pieters C. M., Head J. W., Sunshine J. M., Fischer E. M., Murchie S. L., Belton M., McEwen A., Gaddis L., Greeley R., Neukum G., Jaumann R. and Hoffmann H. (1993) Crustal Diversity of the Moon: Compositional Analyses of Galileo Solid State Imaging Data. *J. Geophys. Res.* **98** (E9), 17127-17148.

Robinson M. S., Hawke B. R., Lucey P. G., and Smith G. A. (1992) Mariner 10 Multispectal Images of the Eastern Limb and Farside of the Moon. *J. Geophys. Res.* **97** (E11), 18265-18274.

Ryder G. (1991) Lunar Ferroan Anorthosites and Mare Basalt Sources: The Mixed Connection. *G. Geophys. Res. Lett.* **18**, 2065-2068.

Schaber G. G. (1973) Lava flows in Mare Imbrium: Geologic evaluation from Apollo orbital photography. *Proc. Lunar Planet. Sci Conf.* **4th**, 73-92.

Shervais J. W. and Taylor L. A. (1985) Apollo 14 Mare Basalts: Petrology and Geochemistry of Clasts from Consortium Breccia 14321. *J. Geophys. Res.* **90** Supplement, C375-C395.

Soderblom L. A., Arnold J. R., Boyce J. M., and Lin R. P. (1977) Regional variations in the lunar maria: Age, remanent magmetism, and chemistry. *Proc. Lunar Planet. Sci Conf.* **8th**, 1191-1199.

Taylor G. J., Warren P., Ryder G., Delano J., Pieters C. and Lofgren G. (1991 a) Lunar Rocks-Appendix: Chemical Data for Lunar Rocks. In *Lunar Sourcebook*

(eds. G. H. Heiken, D. T. Vaniman and B. M. French), pp. 183-284. Cambridge Univ. Press.

Taylor G. J., Warren P., Ryder G., Delano J., Pieters C. and Lofgren G. (1991 b) Lunar Rocks. In *Lunar Sourcebook* (eds. G. H. Heiken, D. T. Vaniman and B. M. French), pp. 183-284. Cambridge Univ. Press.

Taylor S. R. and Jakes P. (1974) The geochemical evolution of the moon. *Proc. Lunar Planet. Sci Conf.* **5th**, 1287-1305.

Taylor S. R. (1982) *Planetary Science: A Lunar Perspective*. Lunar and Planetary Institute, Houston. 481 pp.

Warren P. H. (1985) The magma ocean concept and lunar evolution. *Annu. Rev. Earth Planet. Sci.* **13**, 201-240.

Wilhelms D. E. and McCauley J. F. (1971) *Geologic Map of the Near Side of the Moon*, U. S. Geologic Survey, Map I-703.

Wilhelms D. E. (1987) *The Geologic History of the Moon*, p. 239. U. S. Geologic Survey Professional Paper 1348.

References (Chapter 2)

Antonenko, I., J. W. Head, J. F. Mustard, and B. R. Hawke, Criteria for the detection of lunar cryptomaria, *Earth, Moon and Planets, 56*, 141-172, 1995.

Belton, M. J. S., and the Galileo SSI team., Lunar impact basins and crustal heterogeneity: New western limb and farside data from Galileo, *Science, 255*, 570-576, 1992

Blewett, D. T., B. R. Hawke, P. G. Lucey, G. J. Taylor, R. Jaumann, and P. D. Spudis, Remote sensing and geologic studies of the Schiller-Schickard region of the Moon, *J. Geophys. Res., 100* (E8), 16,959-16,977, 1995.

Blewett, D. T., P. G. Lucey, and B. R. Hawke, Clementine images of the lunar sample-return stations: Refinement of FeO and TiO_2 mapping techniques, *J. Geophys. Res., 102* (E7), 16,319-16,325, 1997.

Eliason, E. M., et al., Digital processing for a global multispectral map of the Moon from the Clementine UVVIS imaging instrument, *Lunar Planet. Sci.* [CD-ROM], *XXX*, abstract 1933, 1999.

Gaddis, L. R., B. R. Hawke, M. S. Robinson, and C. Coombs, Compositional analyses of small lunar pyroclastic deposits using Clementive multispectral data, *J. Geophys. Res., 105* (E2), 4245-4262, 2000.

Giguere, T.A., B. R. Hawke, G. J. Taylor, and P. G. Lucey, Geochemical studies of lunar cryptomare, *Lunar Planet. Sci.* [CD-ROM], *XXIX*, abstract 1782, 1998.

Giguere, T. A., G. J. Taylor, B. R. Hawke, and P. G. Lucey, The titanium contents of lunar mare basalts, *Meteorit. Planet. Sci., 35*, 193-200, 2000.

Hawke, B. R., and J. W. Head, Impact melt on lunar crater rims, in *Impact and Explosion Cratering*, edited by R. O. Pepin, D. J. Roddy, and R. B. Merrill, pp. 815-841, Pergamon, Tarrytown, N.Y., 1977.

Hawke, B. R., D. MacLaskey, and T. B. McCord, Multispectral imaging of lunar crater deposits, *Paper presented to the Conf. On the Lunar Highlands Crust*, 50-52, Lunar and Planet. Inst., Houston, TX, 1979.

Hawke, B. R., and P. D. Spudis, Geochemical anomalies on the eastern limb and farside of the moon, *Proc. Conf. Lunar Highlands Crust,* 467-481, 1980.

Hawke, B. R., and J. F. Bell, Remote sensing studies of lunar dark-halo impact craters: Preliminary results and implications for early volcanism, *Proc. Lunar Planet. Sci. Conf 12B*, 665-678, 1981.

Hawke, B. R., P. D. Spudis, and P. E. Clark, The origin of selected lunar geochemical anomalies: Implications for early volcanism and the formation of light plains, *Earth, Moon, and Planets, 32*, 257-273, 1985.

Hawke, B. R., C. R. Coombs, L. R. Gaddis, P. G. Lucey, and P. D. Owensby, Remote sensing and geologic studies of localized dark mantle deposits on the Moon, *Proc. Lunar Planet. Sci. Conf. 19th*, 255-268, 1989.

Hawke, B. R., T. A. Giguere, P. G. Lucey, C. A. Peterson, G. J. Taylor, and P. D. Spudis, Multidisciplinary studies of ancient mare basalt deposits, *Workshop on New Views of the Moon,* 37-38, Lunar and Planet. Inst., Houston, TX, 1998.

Hawke, B. R., T. G. Giguere, D. T. Blewett, P. G. Lucey, C. A. Peterson, G. J. Taylor, and P. D. Spudis, Remote sensing studies of ancient mare basalt deposits, *Lunar Planet. Sci.* [CD-ROM], *XXX*, abstract 1956, 1999.

Head, J. W., and L. Wilson, Alphonsus-type dark-halo craters: Morphology, morphometry, and eruption conditions, *Proc. Lunar Planet. Sci. Conf. 10th*, 2861-2897, 1979.

Head, J. W., and L. Wilson, Lunar mare volcanism: Stratigraphy, eruption conditions, and the evolution of secondary crusts, *Geochim. Cosmochim. Acta, 56*, 2144-2175, 1992.

Head, J. W., S. Murchie, J. F. Mustard, C. M. Pieters, G. Neukum, A. McEwen, R. Greeley, E. Nagel, and M. J. S. Belton, Lunar impact basins: New data for the western limb and far side (Orientale and South Pole-Aitken basins) from the first Galileo flyby, *J. Geophys. Res., 98* (E9), 17,149-17,181, 1993.

Isbell, C. E., et al., Clementine: A multispectral digital image model archive of the Moon, *Lunar Planet. Sci.* [CD-ROM], *XXX*, abstract 1812, 1999.

Lucey, P. G., G. J. Taylor, and E. Malaret, Abundance and distribution of iron on the Moon, *Science, 268*, 1150-1153, 1995.

Lucey, P. G., D. T. Blewett, and B. R. Hawke, Mapping the FeO and TiO_2 content of the lunar surface with multispectral imagery, *J. Geophys. Res., 103* (E2), 3679-3699, 1998.

Lucey, P. G., D. T. Blewett, G. J. Taylor, and B. R. Hawke, Images of lunar surface maturity, *J. Geophys. Res., 105* (E8), 20,377-20,386, 2000a.

Lucey, P. G., and D. T. Blewett, Lunar iron and titanium abundance algorithms based on final processing of Clementine ultraviolet-visible images, *J. Geophys. Res., 105* (E8), 20,297-20,305, 2000b.

Nozette S., et al., The Clementine mission to the Moon: Scientific overview, *Science, 266*, 1835-1839, 1994.

Robinson, M. S., A. S. McEwen, E. Eliason, E. M. Lee, E. Malaret, and P. G. Lucey, Clementine UVVIS global mosaic: A new tool for understanding the lunar crust, *Lunar Planet. Sci.* [CD-ROM], *XXX*, abstract 1933, 1999.

Schultz, P. H., and P. D. Spudis, Evidence for ancient mare volcanism, *Proc. Lunar Planet. Sci. Conf. 10th*, 2899-2918, 1979.

Schultz, P. H., and P. D. Spudis, Beginning and end of lunar mare volcanism, *Nature, 302*, 233-236, 1983.

Scott, D. H., Geologic map of the Maurolycus quadrangle of the Moon, *U. S. Geol. Surv. Map I-695*, 1972.

Shoemaker, E. M., and R. J. Hackman, Stratigraphic basis for a lunar time scale, in *The Moon – Internat. Astron. Union Symposium 14*, edited by Z. Kopal and Z. Mikhailov, 289-300, 1962.

Shorthill, R. W., and J. M. Saari, Infrared observation on the eclipsed Moon, *Boeing Sci. Research Lab., Doc. D1-82-0778*, 1969.

Smrekar, S., and C. M. Pieters, Near-infrared spectroscopy of probable impact melt from three large lunar highland craters, *Icarus, 63,* 442-452, 1985.

Tompkins, S., and C. M. Pieters, Mineralogy of the lunar crust: Results from Clementine, *Meteorit. Planet. Sci., 34*, 25-41, 1999.

Wilhelms, D. E., and J. F. McCauley, Geologic map of the near side of the Moon, *U. S. Geol. Surv. Map I-703*, 1971.

Wilhelms, D. E., The geologic history of the Moon, *U. S. Geol. Surv. Prof. Pap. 1348*, 1987.

Zisk, S. M., G. H. Pettengill, and G. W. Catula, High-resolution radar map of the lunar surface at 3.8cm wavelength, *Moon*, *10*, 17-50, 1974.

References (Chapter 3)

Adams, J. B. (1974) Visible and near-infrared diffuse reflectance spectra as applied to remote sensing of solid objects in the solar system. *J. Geophys. Res.*, **79**, 4829-4836.

Andre, C. G., Wolfe, R. W., and Adler, I. (1979) Are early magnesium-rich basalts widespread on the Moon? *Proc. Lunar Planet. Sci. Conf. 10th*, 1739-1751.

Antonenko, I., Head, J. W., Mustard, J. F., and Hawke, B. R. (1995) Criteria for the detection of lunar cryptomaria. *Earth, Moon and Planets* **69**, 141-172.

Bell, J. F. and Hawke, B. R. (1984) Lunar dark-haloed impact craters: Origin and implications for early mare volcanism. *J. Geophys. Res.* **89**, 6899-6910.

Blewett, D. T., Hawke, B. R., Lucey, P. G., Taylor, G. J., Jaumann, R., and Spudis, P. D. (1995a) Remote sensing and geologic studies of the Schiller-Schickard region of the Moon. *J. Geophys. Res.* **100** (E8), 16959-16977.

Blewett, D. T., Hawke, B. R., Lucey, P. G., and Spudis, P. D. (1995b) A spectral survey of the Crisium basin region of the Moon. *Geophys. Res. Let.* **22**, 3059-3062.

Blewett, D. T., Lucey, P. G., Hawke, B. R., and Jolliff, B. L. (1997) Clementine images of the sample-return stations: Refinement of FeO and TiO_2 mapping techniques. *J. Geophys. Res.* **102** (E7), 16319-16325.

Blewett, D. T. and Hawke, B. R. (2001) Remote sensing and geological studies of the Hadley-Apennine region of the Moon. *Met. and Planet. Sci.* **36**, 701-730.

Burns, R. G. (1970a) Mineralogical applications of Crystal Field Theory. *Cambridge Univ.,* London. pp. 224.

Burns, R. G. (1970b) Crystal field spectra and evidence of cation ordering in olivine minerals. *Am. Mineral.*, **55**, 1602-1632.

Burns, R. G. (1974) The polarized spectra of iron in silicates: Olivine, a discussion of neglected contributions from Fe ions in M(1) sites. *Am. Mineral.*, **59**, 625-629.

Carr, M. H. (1966) Geologic map of the Mare Serenitatis region of the Moon. *U.S. Geol. Surv. Misc. Geol. Map I-599.*

Carr, M. H. (1969) Geologic map of the Alphonsus region of the Moon. *U.S. Geol. Surv. Misc. Geol. Map I-489.*

Clark, P. E. and Hawke, B. R.(1987) The relationship between geology and geochemistry in the Undarum/Spumans/Balmer region of the Moon. *Earth, Moon, and Planets* **38**, 97-112.

Clark, P. E. and Hawke, B. R. (1991) The lunar farside – The nature of highlands east of Mare Smythii. *Earth, Moon, and Planets* **53**, 93-107.

Davis, P. A. (1980) *J. Geophys. Res.* **85**, 3209.

Eliason, E. M. *et al.* (1999) Digital processing for a global multispectral map of the Moon from the Clementine UV-VIS imaging instrument (abstract). Lunar Planet. Sci. 30, #1933, Lunar and Planetary Institute, Houston, Texas, USA (CD-ROM).

Gaddis, L. R., Pieters, C. M., and Hawke, B. R. (1985) Remote sensing of lunar pyroclastic mantling deposits. *Icarus*, **61**, 461-489.

Giguere, T.A., B. R. Hawke, G. J. Taylor, and P. G. Lucey (1998) Geochemical studies of lunar cryptomare, *Lunar Planet. Sci.* [CD-ROM], *XXIX*, abstract 1782.

Giguere, T. A., Hawke, B. R., Smith, G. A., Taylor, G. J., Blewett, D. T., Lucey, P. G., and Spudis, P. D. (2000) Mafic anomolies in the lunar highlands. *Lunar Planet. Sci. XXXI, abstract no. 1760.*

Giguere, T. A., G. J. Taylor, B. R. Hawke, and P. G. Lucey (2000) The titanium contents of lunar mare basalts, *Meteorit. Planet. Sci.,* **35**, 193-200.

Giguere, T. A., Hawke, B. R., Blewett, D. T., Taylor, G. J., Lucey, P. G., and Spudis, P. D. (2001) Geochemical Studies Of The Lomonosov-Fleming Region Of The Lunar Farside. *Lunar Planet. Sci. XXXII, abstract no. 1516.*

Gillis, J. J., Spudis, P. D. (2000) Geology of the Smythii and Marginis region of the Moon: Using integrated remotely sensed data. *J. Geophys. Res.* **105** (E2), 4217-4233.

Haines, E. L., Etchegaray-Ramireez, M. I., and Metzger, A. E. (1978) Thorium concentrations in the lunar surface. II: Deconvolution modeling and its application to the regions of Aristarchus and Mare Smythii. *Proc. Lunar Planet. Sci. 9th*, 2985-3013.

Hartmann, W. K. (1967) Lunar crater counts, I: Alphonsus. *Commun., 6*, 31-38. Lunar and Planetary Laboratory, Univ. of Arizona, Tucson.

Hartmann, W. K. and Wood, C. (1971) *The Moon* **3**, 3.

Hawke, B. R. and Head, J. W. (1977) Impact melt on lunar crater rims. In *Impact and Explosion Cratering* (D. J. Roddy, R. O. Pepin, and R. B. Merrill, eds.), pp. 815-841. Pergamon, New York.

Hawke, B. R. and Head, J. W. (1977) Impact melt volumes associated with lunar craters (abstract). In *Lunar and Planetary Science X*, pp. 510-512. Lunar and Planetary Institute, Houston.

Hawke, B. R., MacLaskey, D., and McCord, T. B. (1979) Multispectral imaging of lunar crater deposits (abstract). In *Papers Presented to the Conference on the Lunar Highlands Crust*, pp. 50-52. Lunar and Planetary Institute, Houston.

Hawke, B. R., McCord, T. B., and Head, J. W. (1980) Small lunar dark mantle deposits of probable pyroclastic origion. *NASA TM-82385*, pp. 155-157.

Hawke, B. R. and Spudis, P. D. (1980) Geochemical anomalies on the eastern limb and farside of the moon. *Proc. Conf. Lunar Highlands Crust.* 467-481.

Hawke, B. R. and Bell, J. F. (1981) Remote sensing studies of lunar dark-halo impact craters: Preliminary results and implications for early volcanism. *Proc. Lunar Planet. Sci. 12B*, 665-678.

Hawke, B. R., Spudis, P. D., and Clark, P. E. (1985) The origin of selected lunar geochemical anomalies: Implications for early volcanism and the formation of light plains. *Earth, Moon, and Planets* **32**, 257-273.

Hawke, B. R., Coombs, C. R., Gaddis, L. R., Lucey, P. G., and Owensby, P. D. (1989) Remote Sensing and Geologic Studies of Localized Dark Mantle Depostis on the Moon. *Proc. Lunar Planet. Sci. Conf. 19th*, pp. 255-268. Lunar and Planetary Institute, Houston.

Hawke, B. R., Peterson, C. A., Lucey, P. G., Taylor, G. J., Blewett, D. T., Campbell, B. A., Coombs, C. R., and Spudis, P. D. (1993) Remote sensing studies of the terrain northwest of Humorum basin. *Geophys. Res. Let.* **20**, 419-420.

Hawke, B. R., Giguere, T. A., Blewett, D. T., Lucey, P. G., Smith, G. A., Taylor, G. J., and Spudis, P. D. (Submitted) Igneous activity in the southern highlands of the Moon. Submitted to: *J. Geophys. Res.*

Hazen, R. M., Bell, P. M., and Mao, H. K. (1978) Effects of compositional variation on absorption spectra of lunar pyroxenes. *Proc. Lunar Planet. Sci. 9th*, 2919-2934.

Heacock, R. L., Kuiper, G. P., Shoemaker, E. M., Urey, H. C., and Whitaker, E. A. (1966) Ranger 8 and 9, part II: Experimenters' analyses and interpretations. *NASA CR-74894*, 182 pp.

Head, J. W. (1976) Lunar volcanism in space and time. *Rev. Geophys. Space Phys., 14*, 265-300.

Head, J. W. and Wilson, L. (1979) Alphonsus-type dark-halo craters: Morphology, morphometry and eruption conditions. *Proc. Lunar Planet. Sci. Conf. 10th*, pp. 2861-2897.

Head, J. W. and Wilson, L. (1992) Lunar mare volcanism: Stratigraphy, eruption conditions, and the evolution of secondary crusts. *Geochim. et Cosmochim. Acta* **56**, 2144-2175.

Head, J. W., S. Murchie, J. F. Mustard, C. M. Pieters, G. Neukum, A. McEwen, R. Greeley, E. Nagel, and M. J. S. Belton (1993) Lunar impact

basins: New data for the western limb and far side (Orientale and South Pole-Aitken basins) from the first Galileo flyby. *J. Geophys. Res.* **98** (E9), 17149-17181.

Heiken, G., Vaniman, D., French, B. (1991) Lunar Sourcebook: a user's guide to the Moon. *Cambridge Univ. Press*, Cambridge.

Hörz, F. (1978) How thick are lunar mare basalts? *Proc. Lunar Planet. Sci. Conf. 9th*, 3311-3333.

Howard, K. A., and Masursky, H. (1968) Geologic map of the Ptolemaeus quadrangle of the Moon. *U.S. Geol. Surv. Misc. Geol. Map I-566.*

Howard, K. A., and Wilshire, H. G. (1975) Flows of impact melt at lunar craters. *J. Res. U.S. Geol. Surv., 3*, 237-251.

Isbell, C. E. *et al.* (1999) Clementine: A multispectral digital image archive of the Moon (abstract). Lunar Planet. Sci. 30, #1812, Lunar and Planetary Institute, Houston, Texas, USA (CD-ROM).

Lucey, P. G., Spudis, P. D., Zuber, M., and Malaret, E. (1994) Topographic compositional unit on the Moon and the early evolution of the lunar crust. *Science* **266**, 1855-xxxx.

Lucey, P. G., Taylor, G. J., Malaret, E. (1995) Abundance and distribution of iron on the Moon. *Science* **268**, 1150-1153.

Lucey, P. G., Blewett, D. T., and Hawke, B. R. (1998) Mapping the FeO and TiO_2 content of the lunar surface with multispectral imagery. *J. Geophys. Res.* **103**, 3679-3699.

Lucey, P. G., Blewett, D. T., and Jolliff, B. L. (2000a) Lunar iron and titanium abundance algorithms based on final processing of Clementine UV-VIS data. *J. Geophys. Res.* **105** (E8), 20297-20305.

Lucey, P. G., Blewett, D. T., Taylor, G. J., and Hawke, B. R. (2000b) Imaging of lunar surface maturity. *J. Geophys. Res.* **105** (E8), 20377-20386.

Maxwell, T. A. and Andre, C. G. (1981) The Balmer Basin: Regional geology and geochemistry of an ancient lunar impact basin. *Proc. Lunar Planet. Sci. 12th*, 715-725.

McCauley, J. F. (1969) Geologic map of the Alphonsus GA region of the Moon. *U.S. Geol. Surv. RLC Map 15, I-586.*

McCord, T. B., Charette, M. P., Johnson, T. V., Lebofsky, L. A., Pieters, C. M., and Adams, J. B. (1972) Lunar spectral types. *J. Geophys. Res.*, **77**, 1349-1359.

McCord, T. B., Clark, R. N., Hawke, B. R., McFadden, L. A., Owensby, P. D., Pieters, C. M., and Adams, J. B. (1981) Moon: Near-infrared spectral reflectance, a first good look. *J. Geophys. Res.*, **86**, 10,883-10,892.

McGetchin, R. R., Settle, M., and Head, J. W. (1973) *Earth Planet. Sci. Lett.* **20**, 226.

Metzger, A. E. and Parker, R. E. (1979) *Earth Planet. Sci. Lett.* **45**, 155.

Mustard, J. F., Head, J. W., Murchie, S. M., Pieters, C. M., Belton, M. S., and McEwen, A. S. (1992) Schickard Cryptomare: Interaction between Orientale ejecta and pre-basin mare from spectral mixture analysis of Galileo SSI data. *Proc. Lunar Planet. Sci. Conf. 23rd*, 957-968.

Oberbeck, V. R., Morrison, R. H., Hörz, R. H., Quaide, W. L., and Gault, D. E. (1974) Smooth Plains and Continuous Deposits of Craters and Basins. *Proc. 5th Lunar Conf.*, **1**,111-136.

Oberbeck, V. R. (1975) The Role of Ballistic Erosion and Sedimentation in Lunar Stratigraphy. *Rev. Geophys. Space Phys.*, **13**(2), 337-362.

Pieters, C. M., Head, J. W., Sunshine, J. M., Fischer, E. M., Murchie, S. M., Belton, M. S., McEwen, A. S., Gaddis, L. R., Greeley, E., Neukum, G., Jaumann, R., and Hoffmann, H. (1993) Crustal diversity of the Moon: Compositional analyses of Galileo Solid State Imaging data. *J. Geophys. Res.*, **98**(E9), 17,127-17,148.

Nozette, S. *et al.* (1994) The Clementine mission to the Moon: Scientific overview. *Science*, **266**, 1835-1839.

Peterfreund, A. R. (1976) Alphonsus dark-haloed craters: Examples of isolated dark mantle sources (abstract). *EOS Trans. AGU, 57*, 275.

Rhodes, J. M. (1977) Some compositional aspects of lunar regolith evolution. *Phil. Trans. Roy. Soc. London* **A285**, 293-301.

Robinson, M. S., Hawke, B. R., Lucey, P. G., and Smith, G. A. (1992) Mariner 10 multispectral images of the eastern limb and farside of the Moon. *J. Geophys. Res.*, **97**(E11), 18,265-18,274.

Robinson, M. S., McEwen, A. S., Eliason, E., Lee, E. M., Malaret, E., and Lucey, P. G. (1999) Clementine UV-VIS global mosaic: A new tool for understanding the lunar crust (abstract). Lunar Planet. Sci. 30, #1931, Lunar and Planetary Institute, Houston, Texas, USA (CD-ROM).

Ryder, G. and Taylor, G. J. (1976) Did mare-type volcanism commence early in lunar history? *Proc. Lunar Planet. Sci. Conf. 7th*, 1741-1755.

Salisbury, J. W., Adler, J. E. M., and Smalley, V. G. (1968) Dark-haloed crater on the Moon, *Mon. Not. R. Astron. Soc.*, 138, 245-249.

Schaeffer, O. A. and Hussain, L. (1973) Early lunar history: Ages of 2 to 4 mm soil fragments from the lunar highlands. *Proc. Lunar Planet. Sci. Conf. 4th*, 1847-1863.

Schmitt, H. H., Trask, N. J., and Shoemaker, E. M. (1967) Geologic map of the Copernicus quadrangle of the Moon. *U.S. Geol. Surv. Misc. Geol. Map I-515.*

Schultz, P. H. (1976) *Moon Morphology*. Univ. Texas Press, austing, pp. 628.

Schultz, P. H. and Spudis, P. D. (1979) Evidence for ancient mare volcanism. *Proc. Lunar Planet. Sci. Conf. 10th,* 2899-2918.

Schultz, P. H. and Spudis, P. D. (1983) The beginning and end of lunar mare volcanism. *Nature*, 302, 233-236.

Shervais, J. W., Taylor, L. A., and Lual, J. C. (1983) Ancient crustal components in the Fra Mauro breccias. *J. Geophys. Res.* **88**, B177.

Shoemaker, E. M. (1962) Interpretation of lunar crater. In *Physics and Astronomy of the Moon* (Z. Kopal, ec.), pp. 283-359. Academic, New York.

Singer, R. B. (2000) Near-infrared spectal reflectance of mineral mixtures: Systematic combinations of pyroxenes, olivine, and iron oxides. *J. Geophys. Res.* **86**, 7967-7982.

Smrekar, S., and Pieters, C. M. (1985) Near-infrared spectroscopy of probable impact melt from three large lunar highland craters. *Icarus*, 63, 442-452.

Spudis, P. D. (2001) What is the Moon made of? *Science* **293**, 1779-1781.

Spudis, P. D. (1995) Inventory of multiring basins on the moon after the Clementine mission. (abstract), *Meteoritics*, **30**, 5, 582.

Taylor, L. A., Shervais, J. W., Hunter, R. H., and Lual, J. C. (1983) Ancient (4.2 AE) Highlands Volcanism: The Gabbronorite Connection? (abstract) *Lunar Planet. Sci. Conf. 14th*, pp. 777-778.

Tompkins, S., and C. M. Pieters, Mineralogy of the lunar crust: Results from Clementine, *Meteorit. Planet. Sci.*, *34*, 25-41, 1999.

Whitaker, E. A. (1966) The surface of the Moon. In *The Nature of the Lunar Surface* (W. N. Hess, D. H. Menzel, J. A. O'Keefe, eds.), p. 79-98. John Hopkins, Baltimore.

Wilhelms, D. E. and El Baz, F. (1977) Geologic map of the east side of the Moon. U.S.G.S. Map I-948.

Wilhelms, D. E. (1987) *The Geologic History of the Moon*, U.S.G.S. Professional Paper 1348.

Young, R. A., Brennan, W. J., and Wolfe, R. W. (1972) Selected volcanic and surficial features, in *Apollo 16 Prelim. Sci. Rep.*, NASA SP-315, 29-70-29-79.